PHYSICAL REVIEW C **88**, 045501 (2013)

High-precision branching-ratio measurement for the superallowed β^+ emitter ^{74}Rb

R. Dunlop,[1,*] G. C. Ball,[2] J. R. Leslie,[3] C. E. Svensson,[1] I. S. Towner,[4] C. Andreoiu,[5] S. Chagnon-Lessard,[1] A. Chester,[5] D. S. Cross,[5] P. Finlay,[1,†] A. B. Garnsworthy,[2] P. E. Garrett,[1] J. Glister,[2] G. Hackman,[2] B. Hadinia,[1] K. G. Leach,[1] E. T. Rand,[1] K. Starosta,[5] E. R. Tardiff,[2] S. Triambak,[2,6] S. J. Williams,[2] J. Wong,[1] S. W. Yates,[7] and E. F. Zganjar[8]

[1]*Department of Physics, University of Guelph, Guelph, Ontario, Canada N1G 2W1*
[2]*TRIUMF, 4004 Wesbrook Mall, Vancouver, British Columbia, Canada V6T 2A3*
[3]*Department of Physics, Queens University, Kingston, Ontario, Canada K7L 3N6*
[4]*Cyclotron Institute, Texas A&M University, College Station, Texas 77843, USA*
[5]*Department of Chemistry, Simon Fraser University, Burnaby, British Columbia, Canada V5A 1S6*
[6]*Department of Physics, University of Western Cape, P/B X 17 Bellville, 7535, South Africa*
[7]*Departments of Chemistry and Physics & Astronomy, University of Kentucky, Lexington, Kentucky 40506-0055, USA*
[8]*Department of Physics and Astronomy, Louisiana State University, Baton Rouge, Louisiana 70803-4001, USA*

(Received 15 November 2012; revised manuscript received 31 August 2013; published 1 October 2013)

A high-precision branching-ratio measurement for the superallowed β^+ decay of ^{74}Rb was performed at the TRIUMF Isotope Separator and Accelerator (ISAC) radioactive ion-beam facility. The scintillating electron-positron tagging array (SCEPTAR), composed of 10 thin plastic scintillators, was used to detect the emitted β particles; the 8π spectrometer, an array of 20 Compton-suppressed HPGe detectors, was used for detecting γ rays that were emitted following Gamow-Teller and nonanalog Fermi β^+ decays of ^{74}Rb; and the Pentagonal Array of Conversion Electron Spectrometers (PACES), an array of 5 Si(Li) detectors, was employed for measuring β-delayed conversion electrons. Twenty-three excited states were identified in ^{74}Kr following $8.241(4) \times 10^8$ detected ^{74}Rb β decays. A total of 58 γ-ray and electron transitions were placed in the decay scheme, allowing the superallowed branching ratio to be determined as $B_0 = 99.545(31)\%$. Combined with previous half-life and Q-value measurements, the superallowed branching ratio measured in this work leads to a superallowed ft value of 3082.8(65) s. Comparisons between this superallowed ft value and the world-average-corrected $\overline{\mathcal{F}t}$ value, as well as the nonanalog Fermi branching ratios determined in this work, provide guidance for theoretical models of the isospin-symmetry-breaking corrections in this mass region.

DOI: 10.1103/PhysRevC.88.045501 PACS number(s): 23.40.−s, 23.20.Lv, 24.80.+y, 21.10.Tg

I. INTRODUCTION

Superallowed $0^+ \rightarrow 0^+$ Fermi β decays between isospin $T = 1$ nuclear analog states, being relatively insensitive to nuclear structure effects and depending only on the vector part of the weak interaction, offer a unique probe into the electroweak interaction of the Standard Model [1]. For example, the conserved-vector-current (CVC) hypothesis, which predicts the existence of a universal, constant, corrected $\mathcal{F}t$ value for all superallowed β decays, has been confirmed to 1.3 parts in 10^4 [2,3]. The currently adopted world-average-corrected $\overline{\mathcal{F}t} = 3071.81(83)$ s [2] is the average of the 13 most precisely measured superallowed β decays and provides the most precise determination of the weak vector coupling constant G_V. This, in turn, provides the most precise determination of the up-down element of the Cabibbo-Kobayashi-Maskawa (CKM) quark-mixing matrix element $V_{ud} = |G_V/G_F| = 0.97425(22)$ [2], where G_F is the Fermi coupling constant determined from purely leptonic muon decay. Furthermore, the sum of the squares of the top-row matrix elements currently provides the most stringent test of CKM unitarity, which is satisfied to a precision of 0.06% [3].

It should be noted that although 13 of the superallowed ft values have been measured to a precision of better than $\pm 0.3\%$, the dominant uncertainties in many of the corrected superallowed $\mathcal{F}t$ values, and hence, the Standard Model tests, are attributable to theoretical correction terms that are applied to the experimental ft values, viz. [1],

$$\mathcal{F}t \equiv ft(1+\delta_R')(1+\delta_{NS}-\delta_C) = \frac{K}{2G_V^2(1+\Delta_R^V)}, \quad (1)$$

where f is the statistical β-decay rate function which is dependent on the experimental Q_{EC} value, K is a constant, $t = [T_{1/2} \times (1 + P_{EC})]/B_0$ is the partial half-life for the decay to the 0^+ isobaric analog state with half-life $T_{1/2}$, branching ratio B_0, and electron capture probability P_{EC}; δ_R', δ_{NS}, and Δ_R^V are radiative corrections, and δ_C is the isospin-symmetry-breaking correction.

The CVC hypothesis predicts that the bare vector coupling strength of the weak interaction between up and down quarks, G_V, is a constant. However, higher-order radiative terms (QCD and QED loop diagrams) effectively renormalize the coupling strength. The "inner" radiative correction [$\Delta_R^V = 2.361(38)\%$] [4,5] is a nucleus-independent correction that does not perturb the CVC test but is crucial to include in Eq. (1) to determine G_V and, by extension, V_{ud}. Recently, the uncertainty in Δ_R^V has been reduced by a factor of 2 [4] and may continue to be improved via lattice QCD calculations [6]. The transition-dependent correction owing to the exchange of virtual photons between the emitted β particle and the nucleus is given by the "outer radiative" correction δ_R', which is independent of the details of nuclear structure [5,7]. The

*rdunlop@uoguelph.ca
†Present address: Instituut voor Kern-en Stralingsfysica, K, V. Leuven, Celestignenlaan 200D, B-3001 Leuven, Belgium.

nuclear-structure-dependent radiative correction $\delta_{\rm NS}$ contains contributions from both the quenched single-nucleon and the internucleon axial-vector interactions involving Gamow-Teller β decay together with a photon exchange with the outgoing β particle, which flips the nucleon spin [5].

The isospin-symmetry-breaking correction δ_C is required to account for the breaking of isospin symmetry by Coulomb and charge-dependent nuclear forces. Recently, a large number of approaches [2,5,8–15] to the isospin-symmetry-breaking corrections in superallowed β decays has been discussed in the literature and the model-dependent systematic uncertainty associated with the δ_C corrections continues to make a significant contribution to the uncertainty in the world-average-corrected $\overline{\mathcal{F}t}$ value [16].

The $A \geqslant 62$ superallowed β decays are predicted to have the largest isospin-symmetry-breaking terms ($>1\%$) among the $T = 1$ nuclei for which high-precision data are currently available, providing an excellent opportunity to test theoretical approaches in this mass region. Precision ft-value determinations for the $A \geqslant 62$ superallowed decays are, however, complicated by their short half-lives and large $Q_{\rm EC}$ values, resulting in a large number of competing allowed Gamow-Teller β-decay branches and extreme challenges in precisely determining the superallowed branching ratio.

The general approach to measuring high-precision superallowed β-decay branching ratios for the $T_Z = 0$ superallowed emitters, for which the isobaric analog is the ground state of the daughter nucleus, is to subtract from unity the sum of the β-delayed ground-state γ-ray transition intensities in the daughter nucleus. However, the large $Q_{\rm EC}$ value of ^{74}Rb (10.4 MeV) leads to a very large energy window of excited 0^+ and 1^+ states that can potentially be fed by allowed Gamow-Teller and nonanalog Fermi β decays [17]. The "Pandemonium" [18] effect follows, in which the total non-superallowed β-decay intensity is fragmented over a large number of excited states. Depending on the sensitivity of the experiment, many of the subsequent weak γ-ray transitions from these excited states can go unobserved. The combined intensity of these many unobserved γ rays can, however, represent a significant fraction of the total non-superallowed β-decay intensity and severely limit the achievable precision in the determination of the superallowed branching ratio. Our collaboration has developed techniques to address the Pandemonium effect in $A \geqslant 62$ superallowed decays [19–21] by combining detailed β-γ-conversion electron spectroscopy following high-statistics β-decay studies of the superallowed emitters with shell-model calculations of the subsequent γ decay in the daughter nucleus. In this technique low-lying 2^+ states in the daughter nucleus are used as *collector states* for the many weak, and often unobserved, γ-decay branches from highly excited 1^+ states populated in Gamow-Teller β decays. Because the direct β decay to a 2^+ level is a second forbidden process, the population of these collector states, together with the shell-model predictions, enable a rigorous estimate of the corresponding unobserved γ-ray decay directly to the ground state and, hence, a precise determination of the superallowed branching ratio. The method is described in more detail in Sec. III B.

In the present work we report a considerable expansion of the ^{74}Kr level scheme based on the Gamow-Teller and nonanalog Fermi β decays of ^{74}Rb, which provides a precise determination of the superallowed branching ratio, $B_0 = 99.545(31)\%$, for ^{74}Rb β decay. This result agrees with, but is more than a factor of 3 more precise than, a previous measurement at TRIUMF's Isotope Separator and Accelerator (ISAC) [19].

In addition, we directly test the isospin-mixing component of the isospin-symmetry-breaking corrections for the low-lying 0^+ excited states of ^{74}Kr. In shell-model calculations, the isospin-symmetry-breaking correction is typically broken into two parts [1,5]:

$$\delta_C = \delta_{C1} + \delta_{C2}. \tag{2}$$

The δ_{C1} term represents differences in configuration mixing between the isobaric analog parent and daughter states within a truncated shell-model calculation with charge-dependent interactions. The δ_{C2} term corrects for the imperfect radial wave-function overlap of the initial proton and resulting neutron involved in the decay owing to the differing Coulomb interaction experienced by the two particles and differences in their separation energies. Perfect isospin symmetry would imply $\delta_{C1} = \delta_{C2} = 0$ and all Fermi β decays of ^{74}Rb would exclusively populate the analog 0^+ ground state of ^{74}Kr. In addition to the reduction in the superallowed transition matrix element owing to both δ_{C1} and δ_{C2}, the isospin symmetry breaking is manifest through weak Fermi decay branches to the nonanalog 0^+ states in the daughter nucleus associated with components of the δ_{C1} correction. If $2\delta^n_{C1}$ is the square of the Fermi matrix element to the nth nonanalog 0^+ state, then we have the approximate result [5],

$$\delta_{C1} \simeq \sum_n \delta^n_{C1}, \tag{3}$$

which is exact when all of the 0^+ states in the shell-model calculation have the same isospin. The individual δ^n_{C1} components to nonanalog 0^+ states that are energetically accessible via β decay can, in principle, be measured experimentally [22] via

$$\delta^n_{C1} \simeq \left(\frac{f_0}{f_n}\right) B_n, \tag{4}$$

where f_n and B_n are the statistical rate function and the β-decay branching ratio to the nth 0^+ state, respectively. Experimental measurements of these nonanalog branching ratios thus provide stringent tests of the individual components of δ_{C1} predicted by current theoretical approaches, particularly their ability to accurately describe the wave functions of the 0^+ states in the parent and daughter nuclei. These comparisons between the experimental and the theoretical δ^n_{C1} values will lead to a more comprehensive understanding of the required shell-model spaces and ultimately a reduction in the uncertainty of the δ_C corrections for the $A \geqslant 62$ nuclei.

II. EXPERIMENT AND ANALYSIS

A. Experimental facilities and apparatus

The experiment was performed at the ISAC facility [23–25] in Vancouver, Canada. TRIUMF's main cyclotron was used to

produce 98 μA of 500-MeV protons, which were sent to the ISAC facility and impinged on a stack of electrically heated ^{nat}Nb foils. Products of the spallation reactions on the Nb target were surface ionized and extracted as singly charged positive ions. ^{74}Rb ions ($T_{1/2} = 64.776$ ms) [26], of 30 keV energy, were selected using the ISAC online mass separator and sent to the 8π spectrometer [27] at a rate of 6.5×10^3 ions/s. The primary beam contaminant was ^{74}Ga ($T_{1/2} = 8.12$ min) [28,29], which was delivered at 1.2×10^3 ions/s, a factor of 10 lower than in the previous experiment at ISAC [19]. The beam was implanted into an aluminized Mylar tape at the mutual centers of the following: one half of the scintillating electron-positron tagging array (SCEPTAR) [30], containing 10 thin (1.6 mm) plastic scintillators that detected emitted β particles; the 8π spectrometer [27], an array of 20 Compton-suppressed high-purity germanium (HPGe) detectors for detecting γ rays emitted following the β decay of ^{74}Rb; and the pentagonal array of conversion electron spectrometers (PACES), an array of 5 (5 mm thick) Si(Li) detectors used for measuring β-delayed conversion electrons.

SCEPTAR was used to provide efficient β-particle detection to determine the total number of detected ^{74}Rb decays, and the β-γ and β-e^- coincidences also allowed suppression of room background γ rays. Furthermore, the geometry of the SCEPTAR array is such that each scintillating paddle is directly in front of an 8π HPGe detector. This one-to-one correspondance allows for bremsstrahlung created by high-energy β particles striking the delrin absorber in front of the HPGe detectors to be suppressed by vetoing the HPGe detector directly behind the struck SCEPTAR detector.

The experiment was run in a cycled mode to limit the interference of in-beam contaminants and the comparatively long-lived decay chain daughters following the rapid decay of ^{74}Rb. A single cycle consisted of 1.0 s of background counting before the radioactive ion beam (RIB) was implanted into the Mylar tape. The RIB was then continuously implanted into the Mylar tape for 20.0 s. A beam kicker downstream of the mass separator then deflected the RIB and the remaining activity on the tape was counted for a further 2.0 s. Finally, the tape was moved, transporting the remaining activity into a lead-shielded collector box outside of the array, thereby removing the long-lived contaminants and daughter nuclei and allowing the cycle to be repeated.

Each detector stream generated independent triggers in singles mode. Coincidences were reconstructed in the offline analysis from the timing of the SCEPTAR, 8π, and PACES events relative to the start of a cycle determined using individual universal logic modules (ULMs), each consisting of three 32-bit latching scalars, one of which counted pulses from a common high-precision 10 MHz $\pm$ 0.1 Hz temperature-stabilized oscillator, providing a time stamp for every event relative to the start of the cycle with a precision of 100 ns.

B. Analysis of the SCEPTAR β data

In addition to the time relative to the start of a cycle, the total integrated charge from each photomultiplier tube as well as the time between triggers with 0.5 ns precision were recorded for each event that was detected by the SCEPTAR detectors.

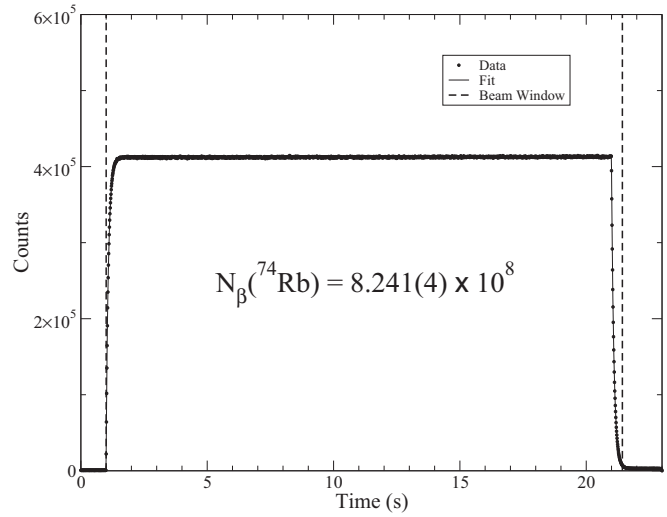

FIG. 1. Fit to the summed β activity for the detected β decays from the 16 857 accepted cycles, with the data binned at 10 ms/channel. The time window used for the "beam-on" analysis is indicated.

A fit to the β activity vs cycle time was performed on a histogram of the β ULM times to determine the number of recorded decays from each radioactive species that was implanted into the tape. To determine these β activities accurately, cycles during which the radioactive beam intensity fluctuated significantly were removed. After this cycle selection, 16 857 of a total of 17 863 cycles, which included $\approx$96% of the total events recorded by the SCEPTAR detectors, were retained for the final analysis.

To determine the total number of detected ^{74}Rb β decays, the sum of the ULM time histograms of the accepted cycles was used (Fig. 1). A dead-time-corrected fit was performed using a maximum-likelihood procedure, which included as free parameters: t_{on}, the time the beam was turned on; t_{off}, the time the beam was turned off; free beam intensity parameters for ^{74}Rb and ^{74}Ga as well as a free constant background rate. The half-life parameters for ^{74}Rb and ^{74}Ga were fixed to their previously measured values of 64.776(43) ms [2] and 8.12(12) min [28,29], respectively.

The fit to these data is shown in Fig. 1 and established a total of $8.241(4) \times 10^8$ ^{74}Rb β decays detected during the "beam-on" analysis window between cycle times of 1.00 and 21.43 s. The quoted uncertainty in the number of detected ^{74}Rb β decays includes a small systematic uncertainty determined by varying the half-lives of ^{74}Rb, ^{74}Ga, and ^{74}Kr within their quoted uncertainties. There was also a small probability that one of the 511-keV annihilation photons emitted following the β^+ decay of ^{74}Rb triggered SCEPTAR. This applies to both the superallowed and non-superallowed β decay branches and does not effect the calculated branching ratios. For the non-superallowed β-decay branches there is, however, also the possibility that an emitted γ-ray or conversion electron triggered SCEPTAR, leading to a cascade-dependent increase in the "β-tagging" efficiency for these non-superallowed β-decay branches. Corrections for this effect were applied to the

measured intensities of the observed γ rays and conversion electrons as described below.

C. Analysis of the 8π γ-ray data

The measured energy, time between triggers, and the ULM time were recorded for each event that was detected by the 8π γ-ray detectors. The absolute time differences between a SCEPTAR event and an 8π event were used to reconstruct β-γ coincidence events, with the requirement that the coincidence time difference be $\leqslant 1.2$ μs.

The relative efficiency of the 8π array as a function of γ-ray energy was measured using sealed ^{133}Ba and ^{152}Eu sources [31]. A RIB of ^{66}Ga was delivered to the 8π immediately following the ^{74}Rb experiment to measure the relative efficiency at high γ-ray energies. The relative γ-ray efficiency curve was fit using the function $\ln(\epsilon) = \sum_{i=0}^{8} a_i (\ln E)^i$, where ϵ is the efficiency of the 8π array at energy E (in MeV) [32]. A calibrated ^{60}Co source with a precisely known activity ($\pm 1.03\%$) was then used to establish the absolute photopeak efficiency of the 8π array as 0.746(8)% at 1332 keV and the absolute γ-ray efficiency curve shown in Fig. 2. These γ-ray efficiency calibrations included corrections for pileup, dead time, and coincidence summing.

Owing to the particular energy difference of 509 keV between the first excited 0^+ state and the ground state in ^{74}Kr, the single escape peak from a γ decay to the ground state was often unresolved from a direct γ-ray transition to the first excited 0^+ state. The energy-dependent single-escape-peak probability was thus carefully measured for the 8π using the ^{66}Ga calibration beam, and used to correct for the single-escape-peak contribution to all γ rays assigned as decays to the 509-keV 0^+ state.

As can be seen in Fig. 3, room background γ-ray transitions dominate the γ-ray singles spectrum owing to the weak nature of the non-superallowed β decay branches of ^{74}Rb. Requiring a coincidence between SCEPTAR and the 8π, however, removes

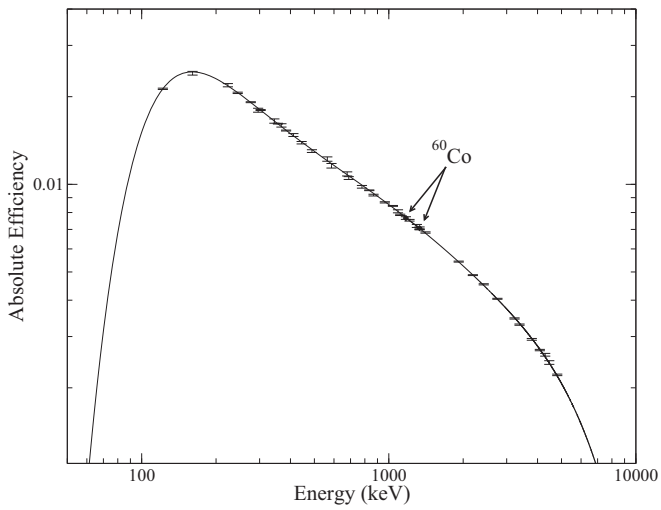

FIG. 2. Absolute γ-ray efficiency curve for the 8π spectrometer. The absolute efficiencies measured using the ^{60}Co source are shown by diamonds.

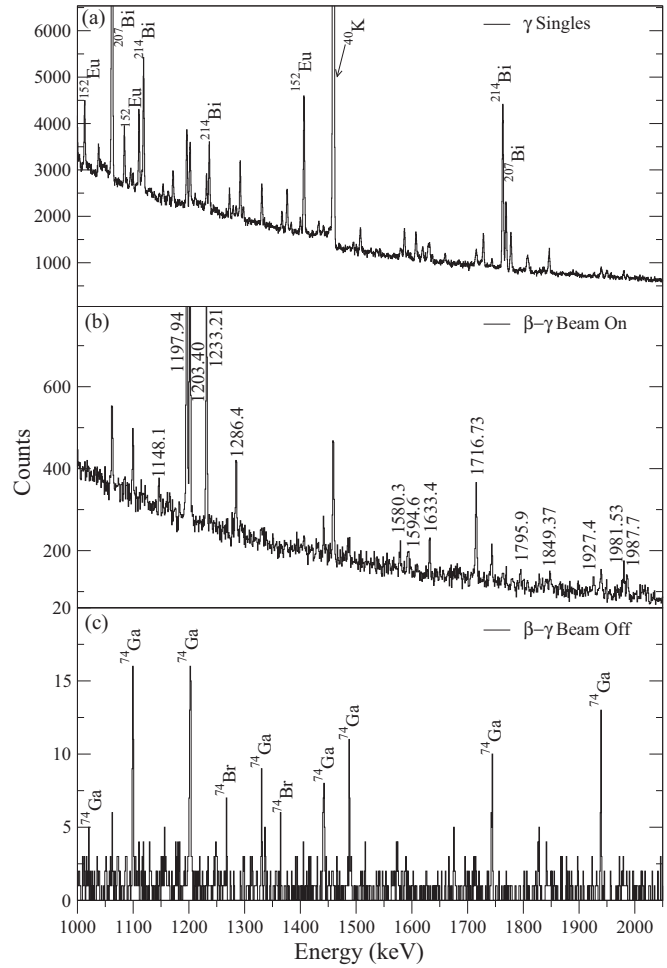

FIG. 3. Portions of the γ-ray spectra between 1000 and 2000 keV. Panel (a) is the raw γ-ray singles spectrum, whereas panels (b) and (c) are bremsstrahlung-suppressed β-γ coincidence spectra. Panel (b) corresponds to the "beam-on" analysis window shown in Fig. 1, whereas panel (c) corresponds to the "beam-off" period outside of this window at the end of the cycle.

these γ rays, while the bremsstrahlung veto discussed above suppresses the bremsstrahlung background from the stopping of the high-energy β^+ particles. To account for the suppressed HPGe detectors, a correction of $C_{\text{Brem}} = N_{8\pi}/(N_{8\pi} - N_S)$ was applied to the γ-ray efficiency, where $N_{8\pi}$ was the number of active HPGe detectors (18 for this experiment) and $N_S = 0.92$ was the average number of SCEPTAR detectors in front of an active HPGe detector that registered a hit per event.

The primary in-beam contaminant, ^{74}Ga, produced a very small β activity compared to ^{74}Rb (see Fig. 1), representing less than 0.3% of the β decays detected during the "beam-on" analysis window. However, the decay of ^{74}Ga yielded a large number of γ-ray branches compared to the very weak nonanalog β-decay branches of ^{74}Rb. A small number of the γ rays that were emitted following the β decay of ^{74}Ga were unresolved from γ rays that were emitted following the decay of ^{74}Rb. To correct for the γ-ray intensity owing to ^{74}Ga decay, a dedicated run was used in which an intense beam of the longer lived ^{74}Ga was intentionally implanted into the Mylar tape. The

area of a contaminating peak relative to the strong 595 keV γ ray from ^{74}Ga decay was used to subtract the contribution of any ^{74}Ga contamination from each γ-ray emitted following ^{74}Rb decay.

The possibility that an emitted γ ray, rather than the β particle of one of the 511-keV annihilation photons, triggered SCEPTAR causing a slight increase in β tagging efficiency for the non-superallowed β decay branches that included at least one subsequent γ ray. For example, the γ-ray detection efficiency for half of the SCEPTAR array was estimated through a GEANT4 Monte Carlo simulation of SCEPTAR to be $\sim$0.8% for the 456-keV γ ray from the first excited state of ^{74}Kr. This leads to a 0.5% β-γ-tagging efficiency increase for other γ rays in coincidence with the 456 keV $2_1^+ \rightarrow 0_{gs}^+$ transition, corresponding to the probability that the 456-keV γ ray triggered SCEPTAR, while the emitted β particle did not. Corrections for this effect were applied to all measured conversion electron and γ-ray intensities, with the largest of these corrections being 1.1% for the 728-keV $2_2^+ \rightarrow 4_1^+$ γ ray, which occurs in a cascade of at least three other γ-ray transitions.

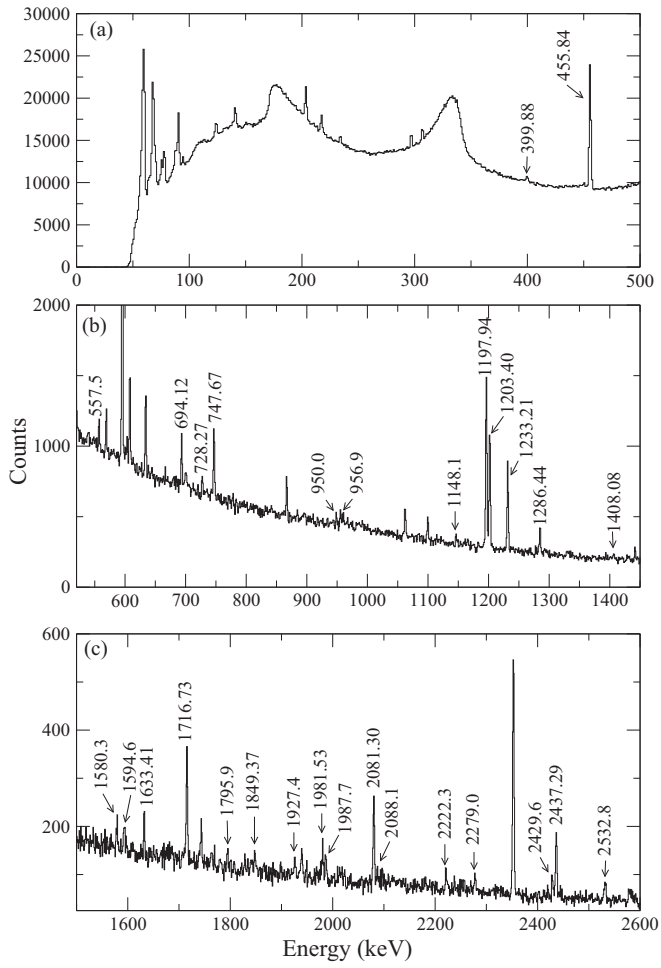

FIG. 4. Identified γ rays in ^{74}Kr following the nonanalog β decay of ^{74}Rb. The labeled peaks were identified as transitions in ^{74}Kr by comparing the β-γ coincidence spectra with the RIB on, to the beam off spectrum [Fig. 3(c)], and a dedicated ^{74}Ga run. Panels (a)–(c) correspond to different portions of the γ-ray spectrum.

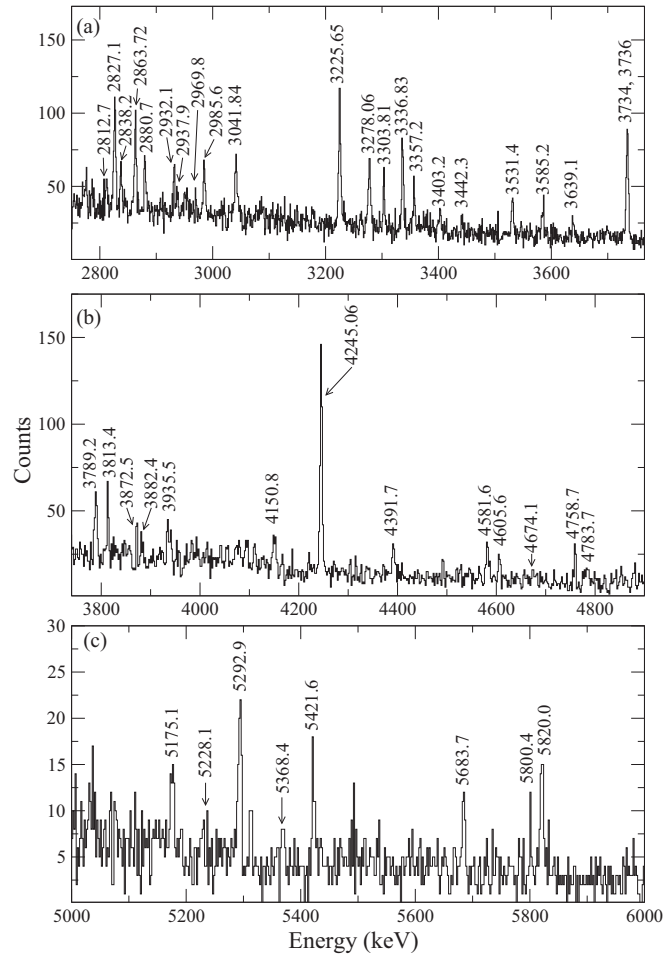

FIG. 5. Identified γ rays in ^{74}Kr following the nonanalog β decay of ^{74}Rb. The labeled peaks were identified as transitions in ^{74}Kr by comparing the β-γ coincidence spectra with the RIB on, to the beam off spectrum [Fig. 3(c)], and a dedicated ^{74}Ga run. Panels (a)–(c) correspond to different portions of the γ-ray spectrum.

A total of 75 γ-ray transitions, shown in Figs. 4 and 5, were identified following the 8.241(4) $\times$ 10^8 detected β decays of ^{74}Rb in this experiment. As discussed below, 58 transitions were placed in the ^{74}Kr decay scheme, to be compared to the 10 transitions identified in previous work [19].

D. Analysis of the PACES conversion-electron data

The first excited 0^+ state of ^{74}Kr at 509 keV excitation energy decays via a highly converted 53-keV $E2$ transition to the first excited 2^+ state or by an $E0$ transition directly to the ground state. To accurately measure the superallowed branching ratio, as well as the nonanalog Fermi decay to this 0^+ state, measurements of these conversion electron intensities with the PACES Si(Li) detector were performed.

The conversion-electron detectors were calibrated using a RIB of ^{80}Rb delivered to the 8π immediately following the ^{74}Rb experiment. The β^+ decay of ^{80}Rb is followed by a 616.8(5)-keV $E2$ transition with a theoretical K-shell

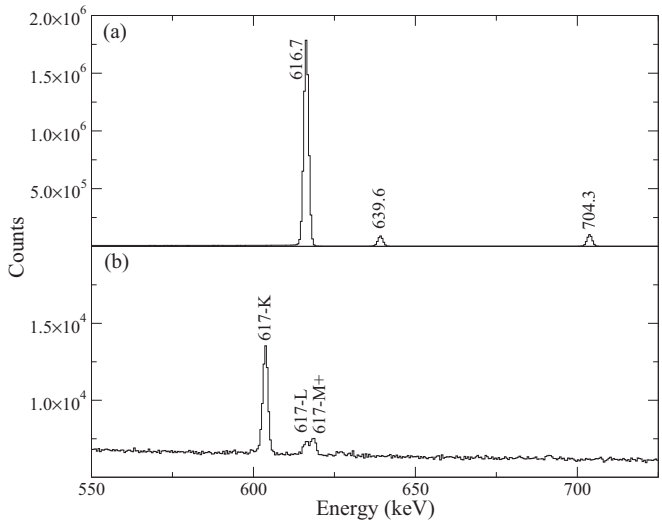

FIG. 6. (a) The ^{80}Rb β-coincident γ-ray energy spectrum and (b) the ^{80}Rb β-coincident conversion electron energy spectrum. The ratio of the 617-keV γ-ray area to the K-conversion electron area was used to determine the absolute efficiency of the PACES conversion-electron detector array to be 3.42(7)%.

conversion coefficient $\alpha_K = 1.527(22) \times 10^{-3}$ [33]. By comparing the detected γ-ray and electron intensities for this transition (see Fig. 6) and using the measured absolute γ-ray efficiency (Fig. 2), the absolute conversion-electron efficiency was, after being corrected for dead time and pileup, found to be the energy-independent value of 3.42(7)% in the region of interest.

Figure 7 shows the conversion-electron energy spectrum recorded in coincidence with β particles detected in SCEPTAR during the ^{74}Rb experiment, while Fig. 8 shows the lower statistics, but very clean conversion-electron spectrum obtained in triple coincidence between PACES, SCEPTAR, and any γ ray of energy $E_\gamma > 511$ keV recorded in the 8π

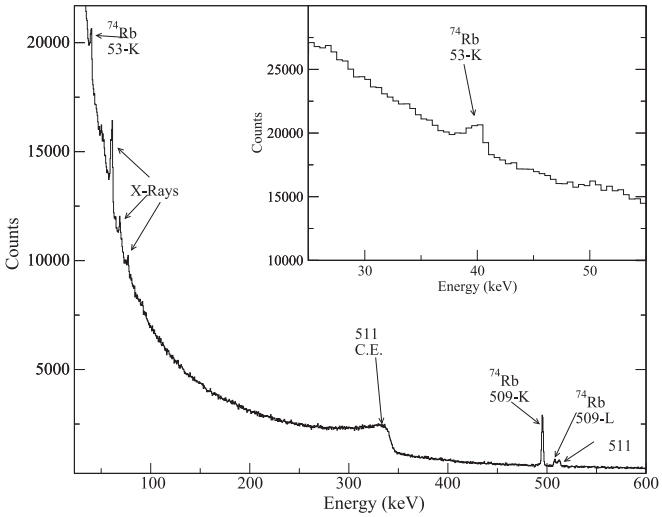

FIG. 7. The β-coincident conversion electron spectrum recorded by the PACES Si(Li) detectors following the β decay of ^{74}Rb. C.E. refers to the Compton edge of the 511 annihilation photons.

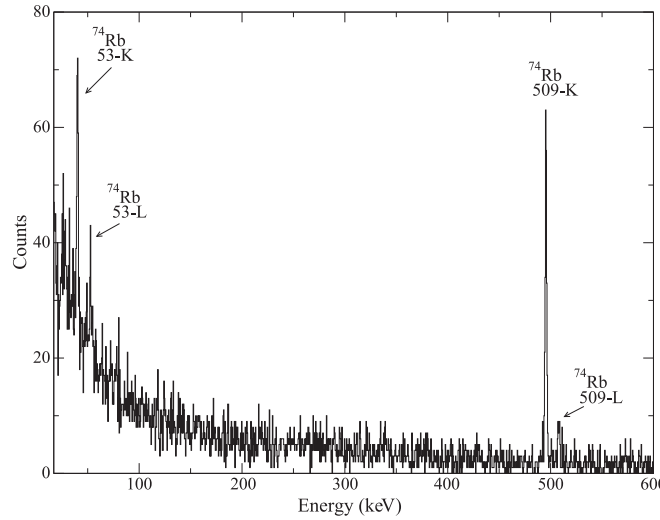

FIG. 8. The β-γ-coincident conversion-electron spectrum recorded by the PACES Si(Li) detectors following the β decay of ^{74}Rb, with a condition that a γ ray of energy $E_\gamma > 511$ keV was detected in coincidence in the 8π spectrometer.

detectors. Internal conversion of both the 53-keV $E2$ and 509-keV $E0$ transitions are clearly identified in both electron spectra.

The intensity of the K-shell conversion electron from the 53-keV $E2$ transition was measured to be $26.5(19) \times 10^{-5}$ per ^{74}Rb β decay. The theoretical ratio of conversion coefficients was calculated [33] yielding $\alpha_{\rm tot}/\alpha_K = 1.268(31)$ and the intensity was also corrected for the small γ-ray contribution using the calculated $\alpha_{\rm tot} = 9.27(16)$. The total intensity of the 53-keV $0_1^+ \rightarrow 2_1^+$ transition was thereby determined to be $37(3) \times 10^{-5}$ per ^{74}Rb β decay. The K-shell intensity of the 509-keV $E0$ transition was measured to be $38.6(9) \times 10^{-5}$ per ^{74}Rb β decay, with the theoretical ratio of electronic factors $\Omega_{L^+}/\Omega_K = 0.141$ [34–36] in excellent agreement with the measured ratio 0.141(7) of the $L+$ to K-shell electron peak areas from Fig. 7. The intensity of the 509-keV $0_1^+ \rightarrow 0_{\rm gs}^+$ transition was thus determined to be $44(3) \times 10^{-5}$ per ^{74}Rb β decay.

The 495-keV K-conversion electron emitted from the decay of the 509-keV excited 0^+ state of ^{74}Kr was also detected by the SCEPTAR plastic scintillator β detectors with the same efficiency as a β particle, leading to an effective increase in the "β"-tagging efficiency for those events in which the 495-keV conversion electron was also emitted. The intensities of the γ rays feeding the 509-keV level were corrected for this effect, while the intensities of the unplaced γ rays were assigned an additional systematic uncertainty to include the possibility that the γ ray may, or may not have, directly fed the 509-keV state.

III. RESULTS

A. ^{74}Kr decay scheme

In this work, 58 γ-ray and conversion-electron transitions originating from 23 excited states populated following ^{74}Rb decay were placed in the ^{74}Kr decay scheme (Fig. 9), representing a significant improvement over the previous study of ^{74}Rb decay in Ref. [19]. The energies and intensities per

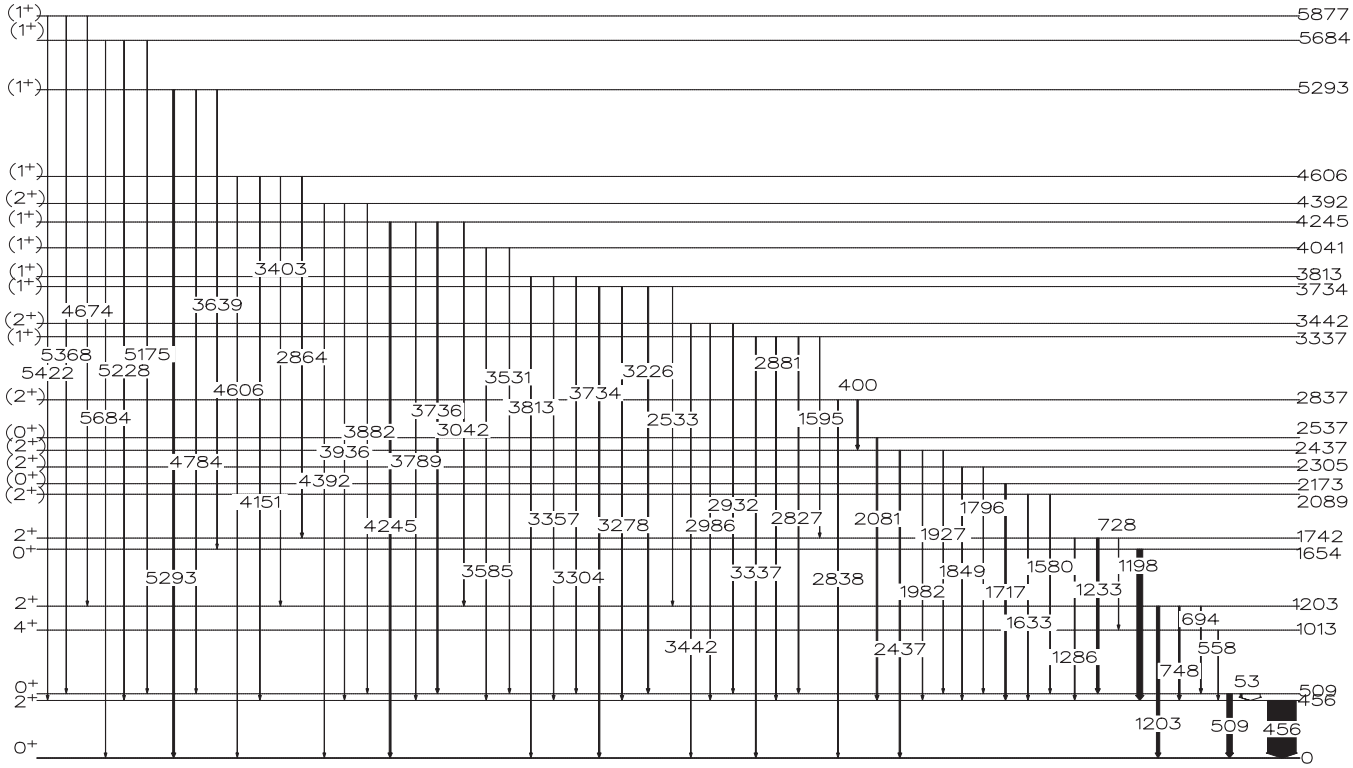

FIG. 9. Decay scheme of ^{74}Kr populated through the β decay of ^{74}Rb as determined in this work. The thicknesses of the arrows represent the relative intensity of the observed transitions.

^{74}Rb β decay of these transitions are listed in Tables I and II. Corrections to the intensities per β decay have been applied for cascade-dependent "β-tagging" efficiency associated with the possibility that a coincident γ-ray or conversion electron, rather than the β particle, triggered the SCEPTAR detector. Our previous studies (see, for example, Fig. 5 of Ref. [21]) have demonstrated a negligible dependence of the SCEPTAR β detector efficiency on Q value for Q_{β^+} values above approximately 1 MeV, corresponding to β decay branches to all excited states in ^{74}Kr below approximately 8.4-MeV excitation energy. No correction to the γ-ray and conversion electron intensities in Tables I and II is therefore required for β Q-value dependence of the SCEPTAR detectors.

The excited states of ^{74}Kr populated in the β decay of ^{74}Rb, as shown in Fig. 9, were determined using γ-ray energy differences as well as γ-γ and γ-e^- coincidences. Figure 10(a), for example, shows the γ rays detected in coincidence with the conversion electrons from the $0_1^+ \rightarrow 2_1^+$ and $0_1^+ \rightarrow 0_{gs}^+$ transitions, while Fig. 10(b) shows the γ-rays detected in coincidence with the 456-keV $2_1^+ \rightarrow 0_{gs}^+$ transition in ^{74}Kr. The current analysis confirms the placement of the 1203- and 4245-keV transitions proposed in Ref. [19]. The precision of the γ-ray and conversion-electron intensities from Ref. [19] have also been improved significantly, as shown in Table III. In addition, the unobserved γ-ray feeding into the 2_1^+ state has been decreased from 1380(180) ppm in Ref. [19] to 649(53) ppm in the current work, a result that has a major influence on the improved precision of the superallowed Fermi branching ratio for ^{74}Rb, as described below. In Table IV we identify a further 17 γ rays emitted following non-superallowed β decay of ^{74}Rb that could not be placed definitively in the level scheme of the ^{74}Kr daughter nucleus.

The spins and parities for the newly observed excited states in ^{74}Kr are important in describing both the non-superallowed β decay and the subsequent γ-ray decay. The observation of new 1^+ states is used to directly measure individual Gamow-Teller β branches. The lowest energy 1^+ state is also used as a parameter in the shell-model calculations described below, which are used to estimate the unobserved γ-ray feeding into the ground state. The assignment of the 2^+ *collector states* is used to estimate the unobserved γ-ray feeding into the ground state. Finally, the observation of 0^+ states is used not only to measure the nonanalog Fermi β decay, but to experimentally constrain the isospin-symmetry-breaking corrections δ_{C1}^n. Assignment of probable spins and parities to the newly observed states is thus required in the determination of the superallowed branching ratio.

The weak population of the excited states in ^{74}Kr following non-superallowed β decay of ^{74}Rb, coupled with the low efficiency of the HPGe detectors at high energies, yielded insufficient γ-γ coincidence data to definitely assign spins and parities to the excited states of ^{74}Kr using a γ-γ angular correlation analysis in this experiment. Nonetheless, information on probable spin-parity assignments could be obtained from the measured γ-ray multiplicities. Rather than requiring full energy photopeaks for high-energy γ rays, where the detection efficiencies were on the order of $\approx$0.2%–0.3%, Compton-scattered events were employed in a γ-ray coincidence multiplicity method to essentially increase the "efficiency" of

TABLE I. Level energies and transition intensities for levels >2.4 MeV. The final column represents the sum of direct β plus unobserved γ-ray feeding of the level. Note that the uncertainty in $I_{\text{out}} - I_{\text{in}}$ differs slightly from the individual I_γ uncertainties added in quadrature owing to common uncertainties in the β and γ calibration data.

E_i (keV)	J_i^π	J_f^π	E_γ (keV)	I_γ (ppm)	$I_{\text{out}} - I_{\text{in}}$ (ppm)
5877.4(7)	(1_9^+)	2_2^+	4674.1(12)	10(4)	41(7)
		0_1^+	5368.4(12)	9(3)	
		2_1^+	5421.6(7)	22(6)	
5683.7(9)	(1_8^+)	0_1^+	5175.1(9)	15(8)	45(8)
		2_1^+	5228.1(16)	13(6)	
		0_{gs}^+	5683.7(9)	18(9)	
5292.9(5)	(1_7^+)	0_2^+	3639.1(6)	18(6)	64(9)
		0_1^+	4783.7(9)	5(4)	
		0_{gs}^+	5292.9(5)	40(6)	
4605.6(8)	(1_6^+)	2_3^+	2863.72(21)	64(7)	134(11)
		2_2^+	3403.2(6)	24(6)	
		2_1^+	4150.8(6)	27(6)	
		0_{gs}^+	4605.6(8)	19(5)	
4391.7(6)	(2_9^+)	0_1^+	3882.4(9)	8(4)	60(11)
		2_1^+	3935.5(5)	26(9)	
		0_{gs}^+	4391.7(6)	27(6)	
4245.06(28)	(1_5^+)	2_2^+	3041.84(27)	65(7)	311(32)
		0_1^+	3736(1)	43(28)	
		2_1^+	3789.2(3)	45(6)	
		0_{gs}^+	4245.06(28)	158(11)	
4041.0(4)	(1_4^+)	0_1^+	3531.4(4)	33(5)	69(8)
		2_1^+	3585.2(4)	35(6)	
3813.4(5)	(1_3^+)	0_1^+	3303.81(27)	32(5)	110(10)
		2_1^+	3357.2(3)	40(6)	
		0_{gs}^+	3813.4(5)	38(6)	
3733.91(24)	(1_2^+)	2_2^+	2532.8(3)	40(7)	276(32)
		0_1^+	3225.65(20)	97(7)	
		2_1^+	3278.06(24)	74(7)	
		0_{gs}^+	3734(1)	64(30)	
3442.3(7)	(2_8^+)	0_1^+	2932.1(3)	26(5)	91(10)
		2_1^+	2985.6(3)	48(7)	
		0_{gs}^+	3442.3(7)	17(5)	
3336.83(22)	(1_1^+)	2_3^+	1594.6(3)	28(5)	230(13)
		0_1^+	2827.1(2)	66(6)	
		2_1^+	2880.7(3)	45(6)	
		0_{gs}^+	3336.83(22)	91(8)	
2837.25(29)	(2_7^+)	(2_6^+)	399.88(15)	104(15)	134(16)
		0_{gs}^+	2838.2(4)	30(6)	
2537.14(12)	(0_4^+)	2_1^+	2081.30(12)	140(8)	140(8)
2437.37(25)	(2_6^+)	0_1^+	1927.4(4)	17(4)	84(19)
		2_1^+	1981.53(25)	43(7)	
		0_{gs}^+	2437.29(14)	128(8)	

TABLE II. Level energies and transition intensities for levels <2.4 MeV. The final column represents the sum of direct β plus unobserved γ-ray feeding of the level. Note that the uncertainty in the $I_{\text{out}} - I_{\text{in}}$ differs from the individual I_γ uncertainties added in quadrature owing to common uncertainties in the β and γ calibration data.

E_i (keV)	J_i^π	J_f^π	E_γ (keV)	I_γ (ppm)	$I_{\text{out}} - I_{\text{in}}$ (ppm)
2305.21(26)	(2_5^+)	0_1^+	1795.9(3)	20(5)	48(7)
		2_1^+	1849.37(26)	28(6)	
2172.58(11)	(0_3^+)	2_1^+	1716.73(11)	141(8)	141(8)
2089.25(19)	(2_4^+)	0_1^+	1580.3(3)	23(4)	73(8)
		2_1^+	1633.41(19)	50(6)	
1742.29(13)	2_3^+	4_1^+	728.27(21)	29(6)	214(14)
		0_1^+	1233.21(8)	195(7)	
		2_1^+	1286.44(13)	83(7)	
1653.78(7)	0_2^+	2_1^+	1197.94(7)	518(12)	499(14)
1203.40(7)	2_2^+	0_1^+	694.12(14)	67(5)	362(18)
		2_1^+	747.67(7)	140(7)	
		0_{gs}^+	1203.40(7)	294(10)	
1013.3(4)	4_1^+	2_1^+	557.5(4)	43(6)	14(9)
509.40(17)	0_1^+	2_1^+	53.23(14)	372(34)	159(58)
		0_{gs}^+	509.40(17)	443(33)	
455.84(4)	2_1^+	0_{gs}^+	455.84(4)	2581(37)	649(53)

the HPGe detectors to a significant fraction of their combined solid angle (≈13%). To do so, a γ-γ coincidence matrix was constructed between HPGe events that were Compton-suppressed vs HPGe events that had no Compton-suppression applied. To remove false γ-ray coincidence events caused by positron annihilation, a gate on all γ rays above 511 keV

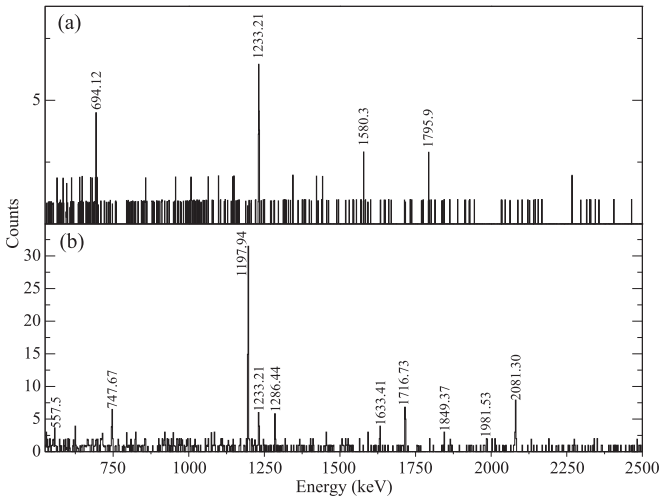

FIG. 10. (a) The γ rays between 525 and 2500 keV in coincidence with (a) the 53-keV $0_1^+ \rightarrow 2_1^+$ and 509-keV $0_1^+ \rightarrow 0_{gs}^+$ conversion-electron transitions and (b) the γ rays in coincidence with the 456-keV $2_1^+ \rightarrow 0_{gs}^+$ γ ray following the β decay of ^{74}Rb.

TABLE III. Comparison of the measured intensities for the γ-ray and conversion-electron transitions that were previously identified in Ref. [19].

Energy (keV)	Intensity	
	Ref. [19] (ppm)	This work (ppm)
53	320(70)	372(34)
509	480(50)	443(33)
456	2500(140)	2581(37)
694	80(50)	67(5)
748	190(50)	140(7)
1198	520(50)	518(12)
1204	260(140)	294(10)
1233	290(40)	195(7)
1286	90(50)	83(7)
4245	120(20)	158(11)

was set on the Compton-unsuppressed events. Bremsstrahlung suppression was also applied to veto events that were actually bremsstrahlung background rather than Compton scattered γ rays. The ratios of the areas of the γ-ray photopeaks in this gated β-Compton-γ coincidence spectrum to the areas in the β-γ coincidence spectrum are related to the average multiplicity of γ rays emitted in coincidence with the γ ray of interest. In cases where the area of the β-Compton-γ photopeak was consistent with 0, a Compton-γ coincidence was used, instead of the full β-Compton-γ coincidence, and corrected for the SCEPTAR efficiency to obtain an upper limit on this ratio. The measured ratios are shown in Fig. 11 for (a) transitions feeding the ground state and (b) transitions feeding the 2_1^+ state at 456 keV. The assigned spins and parities of the levels from which each transition arises are indicated.

TABLE IV. Intensities of the γ rays that were not placed in the level scheme of ^{74}Kr following the decay of ^{74}Rb.

Energy (keV)	I_γ (ppm)
950.0(4)	18(9)
956.9(3)	25(11)
1148.1(3)	25(11)
1408.08(6)	16(9)
1987.7(3)	26(11)
2088.1(5)	19(9)
2222.3(3)	32(12)
2279.0(4)	28(11)
2429.6(3)	37(14)
2812.7(5)	21(10)
2937.9(7)	17(9)
2969.8(10)	10(7)
3872.5(7)	16(8)
4581.6(7)	29(11)
4758.7(7)	25(10)
5800.4(14)	10(6)
5820.0(7)	33(13)

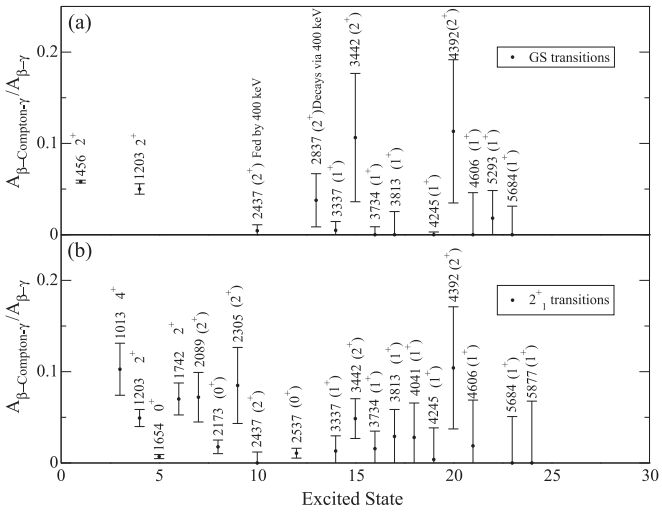

FIG. 11. The ratio of the area of β-Compton-γ coincidences gated on all Compton events above 511 keV to the photopeak area in β-γ coincidence for (a) ground-state transitions and (b) transitions to the first excited 2^+_1 state at 456 keV. Data points shown as diamonds are upper limits based on Compton-γ coincidences corrected for the efficiency of SCEPTAR.

Firm assignments are from Refs. [19,37], while the tentative assignments are based on the multiplicity method described here.

This method exploits the fact that the multiplicity of coincident γ rays should be different for levels differing in spin owing to the β-decay selection rules. The coincident multiplicity for γ rays originating from 2^+ levels should be comparatively large as these levels must be fed by γ rays originating from higher-lying 0^+, 1^+, and 2^+ states, instead of being directly populated by β decay, which is second forbidden and thus negligible. Next, γ rays originating from 0^+ states have lower coincidence multiplicities because these states can be fed by γ decay from 1^+ and 2^+ states, but also potentially have a direct nonanalog Fermi β-feeding component. Finally, γ rays decaying from 1^+ states directly to the ground or 2^+_1 state have almost no coincidence multiplicity above 511 keV as these 1^+ states are largely populated directly by Gamow-Teller β decay rather than γ decay from above. These statements are only general guidelines and the observed transitions are also strongly dependent on the initial and final nuclear wave functions involved. Nonetheless, groupings of the ratios consistent with the above expectations are observed in Fig. 11 and have been used to tentatively assign spins and parities to the newly identified levels in Fig. 9.

For example, the previously known 2^+ states at 456, 1203, and 1742 keV display similar ratios in Fig. 11 clustered around $\approx$0.05. These relatively large ratios are consistent with states that are not accessible by direct β decay but must always be in coincidence with at least one other γ ray, which feeds the state from above. The measured ratio for the 1013-keV 4^+_1 state is approximately twice that of the 2^+ states, as this level is expected to be fed by higher-lying states in a feeding cascade of at least two coincident γ rays. The newly identified levels at 2089 and 2305 keV are consistent with excited (2^+) states because they have high coincidence γ-ray multiplicities and were observed to decay to both the 0^+_1 and the 2^+_2 states.

Although the 2437-keV state appears to have no coincidence multiplicity in Fig. 11, this state is fed from above by a 400-keV γ-ray transition that is removed by the energy gate on the Compton background above 511 keV. The 2437-keV level decays to the 0^+_{gs}, 0^+_1, and 2^+_1 levels, while the 2837-keV level decays to the 0^+_{gs} and (2^+_6) states, consistent with the 2437- and 2837-keV levels having spin-parity (2^+). The levels at 3442 and 4392 keV also have coincident γ-ray multiplicities consistent with (2^+) states and γ decay to the 0^+_{gs}, 2^+_1, and 0^+_1 levels.

Perhaps most interesting is the indication of potential new (0^+) states which provide direct tests of the δ_{C1} isospin-symmetry-breaking-correction components. The 0^+ state at 1654 keV was previously identified in a Coulomb excitation experiment [37], and the similar γ-ray coincident multiplicities of the levels at 2173 and 2537 keV in the current work provide tentative evidence that these are also (0^+) states. These levels were also not observed to decay to any other 0^+ states as these would be γ-forbidden $E0$ transitions, further strengthening the tentative (0^+) assignments for these states.

Finally, the remaining levels that have coincident γ-ray multiplicities consistent with 0 are assigned as tentative (1^+) states. Each of these levels is observed to γ decay to at least one 0^+ state removing the possibility for a 0^+ assignment. However, these states could possibly be weakly fed by low-energy γ-ray transitions from above which do not satisfy the energy gate >511 keV. Given the high-excitation energies of the levels involved, feeding by low-energy γ-ray transitions from above appears less likely than the direct Gamow-Teller β feeding of these states, and tentative spin-parity assignments of (1^+) have thus been made. The first excited (1^+) level is assigned to be at 3337 keV, although this level is not populated as strongly as some of the more highly excited (1^+) levels.

B. Superallowed branching ratio

The superallowed branching ratio for ^{74}Rb decay is determined by subtracting the sum of the ground-state γ-ray and electron transition intensities from unity. The fifth columns of Tables I and II were used to determine the total *observed* ground-state feeding as $I^{obs}_{gs} = 0.395(7)\%$. However, as described in the Introduction, the large Q_{EC} value [$Q_{EC} = 10.4168(39)$] MeV for ^{74}Rb decay leads to to the weak population of a very large number of excited 1^+ states in the daughter nucleus, for which the subsequent γ decay to the ground state may be unobserved and must be accounted for. To perform this correction we consider the measured differences, $I_{out} - I_{in}$, in the γ-ray and conversion electron intensities leaving and entering each excited state of ^{74}Kr, as tabulated in Tables I and II. For 1^+ states, $I_{out} - I_{in}$ is primarily attributable to direct Gamow-Teller β feeding with, perhaps, a small contribution from unobserved γ-ray feeding from above. The observed excess γ-ray intensity leaving a 0^+ state arises, in general, from a combination of direct nonanalog Fermi β feeding and unobserved γ-ray feeding from above. The excited 2^+ states, however, are effectively fed entirely by γ

TABLE V. γ-ray feeding from states above 1742 keV plus direct non-superallowed β feeding to the six lowest 0^+ and 2^+ states in ^{74}Kr. The ground-state feeding is broken into two components: the direct γ-ray feeding 0_{gs}(direct) and the multiple-step feeding 0^+_{gs}(multi) through higher excited 2^+ states. Note that we have attributed the observed feeding of the 4^+_1 level from the 1742-keV 2^+_3 level (14 ppm) to the feeding of the 1742-keV level.

J^π_i	E	Experiment	Theory								
	(keV)	GT + F (ppm)	F (ppm)	GT[a] (ppm)	GT[b] (ppm)	GT[c] (ppm)	GT[d] (ppm)	GT[a] (%)	GT[b] (%)	GT[c] (%)	GT[d] (%)
0^+_{gs}(direct)	0	430(35)		1095	1007	858	2172	24.6	24.5	20.8	23.6
0^+_{gs}(multi)	0	201(12)		166	160	172	418	3.7	3.9	5.6	4.5
2^+_1	456	1440(48)		1598	1470	1450	3240	35.8	35.8	37.2	35.2
0^+_1	509	553(49)	360	721	663	600	1580	16.2	16.1	15.4	17.2
2^+_2	1203	501(14)		433	399	410	870	9.7	9.7	10.5	9.5
0^+_2	1654	518(13)	228	217	199	200	460	4.9	4.8	5.1	5.0
2^+_3	1742	306(10)		228	210	210	460	5.1	5.1	5.4	5.0
Total		3949(70)	588	4458	4108	3900	9200	100	100	100	100

[a]Lowest 1^+ Level at: 3.337 MeV, $g_{A_{\rm eff}} = 0.75$.
[b]Lowest 1^+ Level at: 3.337 MeV, $g_{A_{\rm eff}} = 0.72$.
[c]Lowest 1^+ Level at: 3.600 MeV, $g_{A_{\rm eff}} = 0.80$.
[d]Lowest 1^+ Level at: 3.200 MeV, $g_{A_{\rm eff}} = 1.00$.

decay from above with an entirely negligible second-forbidden β-feeding component. The combined excess γ-ray intensity observed leaving the three lowest-lying 2^+ states, $I'_{2^+_{1,2,3}} = 649(53) + 362(18) + 214(14) = 1225(57)$ ppm, is thus a direct measurement of the total unobserved γ-ray feeding from above into these low-lying 2^+ states and, as noted in the Introduction, can be combined with shell-model calculations to estimate the unobserved γ feeding to the ground state.

We define $\overline{B}_{gs}$ as the ratio of the γ-ray intensity I'_{gs} from the unobserved weakly populated levels that proceeds to the ground state without passing through one of the low-lying 2^+ collector states to the total γ-decay intensity from these levels $(I'_{gs} + I'_{2^+})$,

$$\overline{B}_{gs}(2^+) = \frac{I'_{gs}}{I'_{gs} + I'_{2^+}}, \tag{5}$$

where I'_{2^+} is the γ-ray intensity from these unobserved levels that does pass through the 2^+ collector states. An estimate of the ratio $\overline{B}_{gs}(2^+)$ through either experimental or theoretical methods, combined with the experimentally measured quantity I'_{2^+}, thus provides an estimate of the desired unobserved ground-state feeding I'_{gs} via

$$I'_{gs} = \frac{I'_{2^+}\overline{B}_{gs}(2^+)}{1 - \overline{B}_{gs}(2^+)}. \tag{6}$$

Table V presents the γ-ray feeding to the first six 0^+ and 2^+ states in ^{74}Kr from the states above 1742 keV plus the direct β feeding to these states and is compared with the results of the shell-model calculations discussed below. The γ-ray intensity feeding the ground state is broken into two components: (i) the γ-ray transitions directly from the Gamow-Teller-fed 1^+ states and (ii) the intensity collected following a multistep γ-decay cascade. The majority of the smaller, multistep γ-ray feeding component to the ground state is likely to have been collected in the significant number of 2^+ states above 1742 keV that are assigned in the current work. Therefore, to estimate the unobserved γ-ray feeding directly to the ground state, we remove the small contributions of the multistep γ cascades from the 2^+_4-2^+_9 levels before calculating $\overline{B}_{gs}$. In the following sections we provide a detailed description of various estimates of $\overline{B}_{gs}(2^+)$ and, thus, the unobserved component of the γ-ray intensity to the ground state.

1. *Experimental estimate of I'_{gs}*

The observed γ-ray feedings into the ground and first excited 2^+ state from all of the states above 1742 keV were 631 and 791 ppm, respectively. Using the same average branching ratio for the observed and unobserved γ-ray transitions to the ground state and first excited 2^+ state, $R = 631/791 = 0.797$, we obtain a first experimental estimate of $\overline{B}_{gs}(2^+_1) = 0.444$ and $I'_{gs} = 517$ ppm. As noted above, multistep γ-ray feeding from above the 1742-keV state is likely to have been collected and observed. Therefore, we remove the observed multistep feeding intensities from the average branching ratio (195 and 201 ppm to the ground and 2^+_1 states, respectively) and obtain a second set of purely experimental estimates, $R = 430/596 = 0.720$, $\overline{B}_{gs}(2^+_1) = 0.419$ and $I'_{gs} = 467$ ppm.

To avoid possible structure-dependent effects associated with using only the first excited 2^+ state as a collector state, we repeat the above estimates using the first three excited 2^+ states as collector states, $R = 631/1023 = 0.617$, $\overline{B}_{gs}(2^+_{1,2,3}) = 0.382$. This gives $I'_{gs} = 756$ ppm, while subtracting the multistep γ-ray feeding gives $\overline{B}_{gs}(2^+_{1,2,3}) = 0.342$ and an estimate of the unobserved ground-state intensity of $I'_{gs} = 636$ ppm. We adopt 636 ppm as our best estimate for the unobserved ground-state γ-ray feeding from this purely experimental branching-ratio method.

2. *Theoretical estimate of I'_{gs}*

To further explore the estimate of $\overline{B}_{gs}$, we have performed shell-model calculations [19,38], for the β decay of ^{74}Rb and the subsequent γ-decay cascades in ^{74}Kr. The first of these calculations was adjusted to reproduce the observed position of the first excited 1^+ state in ^{74}Kr at 3.337 MeV and the effective Gamow-Teller strength was quenched to $g_{A_{\rm eff}} = 0.75$ to accurately reproduce the total emitted γ-ray intensity from the sum of the first three excited 2^+ states in ^{74}Kr. This was done in an attempt to average any state-by-state discrepancies in the observed intensities of the collector states with those predicted by the shell-model calculation. The calculated γ-ray feeding from states above 1742 keV is shown for the six lowest 0^+ and 2^+ states in ^{74}Kr in Table V.

Using this $g_{A_{\rm eff}} = 0.75$ shell-model calculation, the predicted total multistep feeding to the ground state that bypasses the low-lying 2^+ and 0^+ states is 166 ppm, in reasonable agreement with the 201(12) ppm observed experimentally from the γ-ray decay of the (2^+) states above 1742 keV. This suggests, as noted above, that essentially all of the multistep component of the γ-decay from the unobserved 1^+ states to the ground state is accounted for in the decay of the many (2^+) states above 1742 keV observed in this work. The average branching ratio $\overline{B}_{gs}(2^+)$ was thus calculated as the β-feeding-weighted γ-ray branching ratios for the direct γ-decay to the ground state and γ-decay to the three lowest-lying 2^+ states from each of the individual 1^+ states in the calculation. The resulting theoretical estimate for the average branching ratio is $\overline{B}_{gs}(2^+_{1,2,3}) = 0.326$, and the corresponding estimate for the unobserved ground-state γ-ray intensity is $I'_{gs} = 594$ ppm, very similar to the estimates from the independent, and purely experimental, branching-ratio method described above.

3. *Reproducing the 2^+_1 γ-ray intensity*

By adjusting the effective Gamow-Teller strength to $g_{A_{\rm eff}} = 0.72$, we were able to reproduce the total collected γ-ray intensity of the first 2^+ state, rather than the first three 2^+ states. The unobserved intensity into the 2^+_1 state was measured to be $I'_{2^+_1} = 649(53)$. Combining this with the shell-model calculation we obtain $\overline{B}_{gs}(2^+_1) = 0.407$ and $I'_{gs} = 444$ ppm. If we now use the measured intensity collected in the first three excited 2^+ states, but use the γ-ray branching ratios calculated using the $g_{A_{\rm eff}} = 0.72$ calculation we obtain, just as in the $g_{A_{\rm eff}} = 0.75$ case, $\overline{B}_{gs}(2^+_{1,2,3}) = 0.326$ and $I'_{gs} = 593$ ppm. A summary of the unobserved intensities predicted using each of these methods is shown in Table VI.

4. *Testing the shell-model parameter space*

To investigate the robustness in the value of $\overline{B}_{gs}(2^+)$ obtained from these shell-model calculations, two previous sets of shell-model calculations were also considered. The calculations of Ref. [19] were performed by setting the first excited 1^+ state at 3.6 MeV, with the effective Gamow-Teller strength quenched to $g_{A_{\rm eff}} = 0.80$. This calculation resulted in an estimate for $\overline{B}_{gs}(2^+_{1,2,3}) = 0.293$ and an estimate of the unobserved ground-state γ-ray intensity of $I'_{gs} = 508$ ppm.

TABLE VI. A summary of the unobserved direct ground-state γ-ray intensities estimated experimentally and by using each of the shell-model calculations. For each calculation we present the results from using 2^+_1 and $2^+_{1,2,3}$ as collector states.

Method	$\overline{B}_{gs}$		I'_{gs} (ppm)	
	2^+_1	$2^+_{1,2,3}$	2^+_1	$2^+_{1,2,3}$
Experiment	0.419	0.342	467	636
$g_{A_{\rm eff}} = 0.75$	0.407	0.326	444	594
$g_{A_{\rm eff}} = 0.72$	0.407	0.326	444	594
$g_{A_{\rm eff}} = 0.80$	0.372	0.293	384	508
$g_{A_{\rm eff}} = 1.00$	0.401	0.322	435	582

The original calculation of Ref. [38] placed the first excited 1^+ state at 3.2 MeV and set the Gamow-Teller strength at $g_{A_{\rm eff}} = 1.00$, resulting in $\overline{B}_{gs}(2^+_{1,2,3}) = 0.322$ and $I'_{gs} = 582$ ppm. Each of these calculations predict quite different absolute Gamow-Teller β feeding, as shown in Table V. However, the ratio of the γ-ray feeding into the first three excited 2^+ states to the direct ground-state feeding summed over the large number of 1^+ states remains relatively insensitive to the details of the calculation, providing very similar estimates of $\overline{B}_{gs}(2^+_{1,2,3})$ and thus I'_{gs}. This highlights the importance of using the calculated ratio $\overline{B}_{gs}$, rather than the predicted absolute γ-ray intensities, as the γ-ray branching ratios remain largely unchanged within the plausible parameter space with no requirement that the shell-model calculations accurately describe the absolute Gamow-Teller feeding. For instance, these four shell-model calculations provide vastly different estimates of the total Gamow-Teller β feeding, 3900–9200 ppm, but the average γ-ray branching ratio to the ground state remains largely unchanged across the parameter space, with $\overline{B}_{gs}(2^+_{1,2,3})$ varying between 0.293 and 0.326 and I'_{gs} consistently within the range of 508–594 ppm, in reasonable agreement with our purely experimental estimate of 636 ppm.

5. *Assignment of an uncertainty to I'_{gs}*

To be conservative in our estimate of the uncertainty in the unobserved ground-state γ-ray intensity, we also consider one additional, purely experimental, approach to the determination of $\overline{B}_{gs}$ and the missing ground-state γ-ray intensity. If we were to consider the nine observed (1^+) states as representative of the complete set of 1^+ states, the average (unweighted by β feeding) of the $\overline{B}_{gs}(2^+)$ values for these observed (1^+) states may be used to estimate the average branching ratio for the unobserved 1^+ states. The fifth columns of Tables I and II were used to determine the experimental $\overline{B}_{gs}(2^+_{1,2,3}) = 0.41(11)$ for the observed 1^+ states, where the quoted uncertainty is the uncertainty in the mean. Combining this branching ratio with the experimental $I'_{2^+_{1,2,3}} = 1225(57)$ ppm, we then arrive at an additional estimate for the unobserved γ feeding to the ground state of $I'_{gs} = 848^{+474}_{-325}$ ppm that is somewhat larger, but consistent with, the best estimates of 593 and 636 ppm obtained from the shell-model calculations and experimental ratio methods described above.

However, we note that B(GT) and $B(M1)$ for the subsequent γ-decay to the ground state of ^{74}Kr are approximately

related via an isospin rotation. In other words, the 1^+ states with the largest B(GT) values for the Gamow-Teller β decay of the ^{74}Rb 0^+ ground state, are also the states with the largest $B(M1)$ values for γ decay to the ground state in ^{74}Kr. As the states with larger B(GT) are more likely to be observed experimentally, this correlation biases the observed ground-state branching ratio towards larger values of $\overline{B}_{\rm gs}$. The average of the observed values of $B_{\rm gs}(2^+_{1,2,3}) = 0.41(11)$ from the nine observed (1^+) states is thus almost certainly an overestimate of the average $\overline{B}_{\rm gs}(2^+_{1,2,3})$ that applies to the large number of very weakly populated and unobserved 1^+ states in ^{74}Kr. We therefore adopt the smaller value of $\overline{B}_{\rm gs}(2^+_{1,2,3}) = 0.33$ from the average of our "best" experimental $\overline{B}_{\rm gs}(2^+_{1,2,3}) = 0.342$, and "best" shell-model $\overline{B}_{\rm gs}(2^+_{1,2,3}) = 0.326$, estimates. However, to be conservative we adopt the ± 0.11 uncertainty in the mean from the determination of $\overline{B}_{\rm gs}(2^+_{1,2,3})$ values from the nine observed (1^+) states, to arrive at an adopted $\overline{B}_{\rm gs}(2^+_{1,2,3}) = 0.33(11)$ for the unobserved weakly populated 1^+ states. We note that this value also encompasses the central value of $\overline{B}_{\rm gs}(2^+_{1,2,3}) = 0.41$ for the nine observed (1^+) states that are expected to have larger-than-average $B_{\rm gs}$ values. Symmetrizing the uncertainty range on $I'_{\rm gs}$, we therefore obtain a conservative estimate of the unobserved γ decay to the ground state of $I'_{\rm gs} = 600(300)$ ppm.

Finally, it should be noted that β-delayed α decay of ^{74}Kr to ^{70}Se is energetically possible for excitation energies in ^{74}Kr above 2.83 MeV. Such α decay of excited states in ^{74}Kr would represent an additional unobserved decay component that must be accounted for in the determination of the superallowed branching ratio. Based on the Q value, the dominant α decay from excited 0^+ and 2^+ states in ^{74}Kr would feed the 0^+ ground state of ^{70}Se via $l = 0$ and $l = 2$ α decay, respectively. However, based on a simple semiclassical estimate of α decay rates [39] in ^{74}Kr competing with a single, 1 Weisskopf unit (W.u.), $E2$ γ-ray transition to either the ground state or first excited 2^+ state of ^{74}Kr, we estimate that γ decay will completely dominate over α decay for excitation energies $\lesssim$8 MeV in ^{74}Kr. It is extremely unlikely that a 2^+ state, which must be γ fed from above, is populated at such high excitation energies in ^{74}Kr following ^{74}Rb β decay ($Q_{\beta^+} = 9.4$ MeV). There is also no expectation of significant isospin mixing with such highly excited 0^+ states in ^{74}Kr that would generate non analog Fermi β decay branches to these states. The other possibility for β-delayed α decay of ^{74}Kr is from highly excited 1^+ states. In this case, decay to the 0^+ ground state of ^{70}Se is angular-momentum/parity forbidden, and α decay would thus be expected predominantly to the first excited 2^+ state in ^{70}Se at 945 keV. We estimate that α decay of these excited 1^+ states would not compete significantly with γ decay for excitation energies in ^{74}Kr $\lesssim 9$ MeV. Furthermore, the 2^+ state of ^{70}Se would then decay to the ground state via a 945-keV and the upper limit on the intensity of this γ-ray in our data was measured to be <7 ppm. The possibility of β-delayed α emission from highly excited states of ^{74}Kr is thus considered to be entirely negligible in comparison with the ± 300 ppm conservative uncertainty assigned to our estimate, 600(300) ppm, of the unobserved γ feeding to the ground state of ^{74}Kr.

Adding the above estimate of the unobserved γ-decay to the ground state of 600(300) ppm to the experimentally observed ground-state feeding of 0.395(7)%, the non-superallowed branching ratio in ^{74}Rb decay is determined in this work to be 0.455(31)%, which is in excellent agreement with the value of 0.4696% from the shell-model calculation with $g_{A_{\rm eff}} = 0.72$ and the first 1^+ state at the observed energy of 3337 keV. We thus arrive at a superallowed branching ratio of $B_0 = 99.545(31)$%, which is in good agreement with, but a factor of 3 more precise than, the only previous precision measurement of this quantity, 99.5(1)% [19]. Although these two measurements, both performed at ISAC, employed different experimental apparatus and are statistically independent, both analyses used similar shell-model calculations for $\overline{B}_{\rm gs}$ to estimate the unobserved ground-state γ-ray intensity $I'_{\rm gs}$. As it is the uncertainty in $\overline{B}_{\rm gs}$ that dominates the final uncertainty in the superallowed branching ratio, we do not take a weighted average of the above results, but rather supersede the earlier work of Ref. [19] with the higher statistics and more precise branching-ratio measurement reported here.

C. Half-life of the 509-keV isomeric 0^+_1 state in ^{74}Kr

The SCEPTAR plastic scintillator detectors were not only sensitive to the detection of β particles but were also sensitive to the β-delayed conversion electrons emitted from the 509-keV isomeric 0^+_1 state in ^{74}Kr. To measure the half-life of this isomeric state, gates were placed on the most intense γ rays at 694, 1233, 2827, and 3226 keV that feed the 509-keV state, while a second set of gates were placed on the 748-, 1198-, and 2437-keV γ rays that directly feed the ground state. Figure 12 shows the resulting time difference spectra between coincident hits in two different SCEPTAR detectors associated with each of these combinations of gates. The spectrum gated on γ-ray transitions feeding the 509-keV level shows a clear exponential decay component owing to the lifetime of the 509-keV level, compared to the prompt β-scattering between SCEPTAR detectors shown in the spectrum gated on the γ-ray transitions bypassing the 509-keV level. The background in the spectrum gated on the ground-state transitions arises from a small number of events within the γ-ray gates from Compton scattered γ-rays that fed the 509-keV state. The data in Fig. 12(b) were fit using an exponential decay plus a constant background to determine the 509-keV-state lifetime. To exclude the prompt peak in which the β particle scattered between two SCEPTAR detectors, the start of the fit was increased until a consistent value for the half-life was obtained, as shown by the points with error bars in Fig. 12(c). We thereby measure the half-life of the 509-keV state to be 14.2(10) ns, in reasonable agreement with a previous measurement of 13.0(7) ns [40]. Combining our half-life with the branching ratio of the 509-keV transition [54(4)%], the partial half-life of the 509-keV $E0$ transition was determined to be 26(3) ns. From this half-life, the $E0$ matrix element $\rho(E0)$ for the $0^+_1 \rightarrow 0^+_{\rm gs}$ decay can be calculated,

$$\rho^2(E0) = \left[\frac{t_{1/2}}{\ln(2)} \sum_j \Omega_j(Z, K) \right]^{-1}, \qquad (7)$$

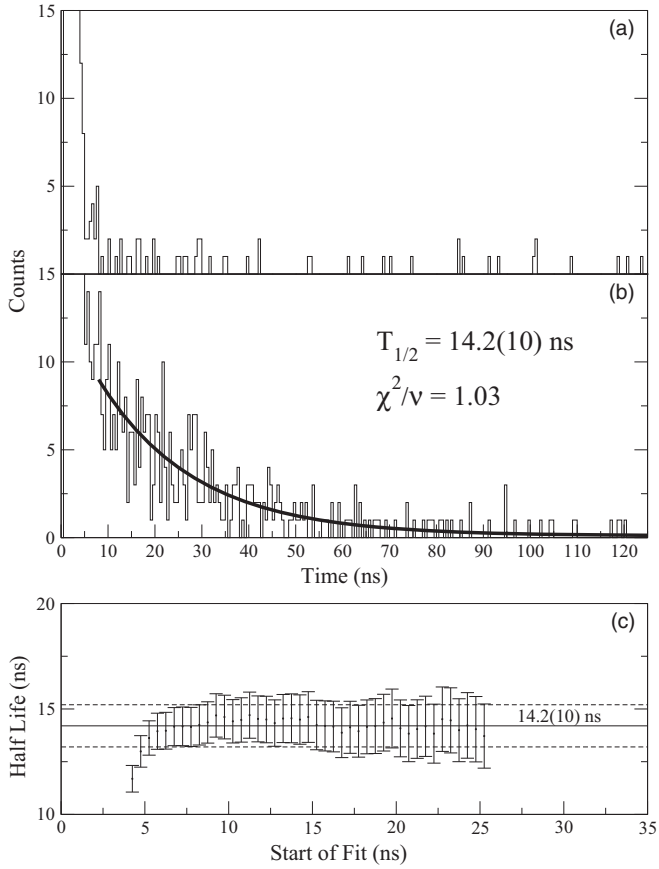

FIG. 12. (a) The time difference between two SCEPTAR hits in the same event gated on the 748-, 1198-, and 2437-keV γ rays feeding the ground state, and (b) gated on the 694-, 1233-, 2827-, and 3226-keV γ rays feeding the 509-keV level. (c) To exclude false coincidences in the "prompt" peak, which arise from β particles scattering from one detector to another, the start of the half-life fit was increased until a consistent value of 14.2(10) ns for the half-life was obtained using 8 ns as the first bin in the fit.

where $\Omega_j(Z,K)$ is the electronic factor for the jth atomic orbital, the sum of which is calculated to be 3.00×10^8 s^{-1} [34–36]. This yields an experimental monopole strength of $\rho^2(E0) = 0.088(9)$, to be compared with the value of 0.085(19) determined in Ref. [40]. It should be noted that the increased precision in ρ^2 in the current work is almost entirely attributable to the increased precision in the branching ratio for the $E0$ decay of the 0_1^+ state.

IV. DISCUSSION

A. ^{74}Rb ft and $\mathcal{F}t$ values and a test of δ_C

Recent measurements of the charge radius and mass of ^{74}Rb, in addition to the superallowed branching ratio reported here, have aimed to reduce the uncertainty in the superallowed $\mathcal{F}t$ value. A recent mass measurement at TRIUMF [41], combined with a previous measurement at ISOLTRAP [42,43], leads to an average $Q_{\rm EC}$ value of 10 416.8(3.9) keV, resulting in a statistical rate function of $f = 47\,283(94)$ [41]. From the ^{74}Rb half-life of $T_{1/2} = 64.776(43)$ ms [2], which is the average of the measurements of Refs. [26,44], the electron capture fraction $P_{\rm EC} = 0.194\%$ [2], and the new superallowed branching ratio of $B_0 = 99.545(31)\%$ reported here, a ^{74}Rb superallowed ft value of $3082.8(10)_{B_0}(20)_{T_{1/2}}(61)_f$ s $= 3082.8(65)$ s is determined. The statistical rate function f, determined from the Q value, currently dominates the uncertainty. However, it is expected that the uncertainty in the Q value will be decreased by approximately an order of magnitude to ~0.5 keV in the near future [41], dramatically lowering the uncertainty in the ft value and fully exploiting the new high-precision branching ratio measurement reported here. At that time, the precision of the experimental ft value for ^{74}Rb decay will approach those of the well measured cases among the sd and $f_{7/2}$ shell nuclei and will become limited by the ±0.07% precision of the current world-average half-life.

A recent measurement of the charge radius of ^{74}Rb has also been performed at TRIUMF, reducing the uncertainty in the Woods-Saxon δ_{C2} value by approximately 20% from $\delta_{C2} = 1.50(30)\%$ to $\delta_{C2} = 1.50(23)\%$ [45]. Using the nucleus-dependent corrections $\delta'_R = 1.50(12)\%$, $\delta_{\rm NS} = -0.075(30)\%$, and $\delta_{C1} = 0.130(60)\%$ [5], the superallowed $\mathcal{F}t$ value of ^{74}Rb becomes $\mathcal{F}t_{\rm WS} = 3075.7(65)_{ft}(36)_{\delta'_R}(9)_{\delta_{\rm NS}}(74)_{\delta_C}$ s $= 3076(11)$ s. The superallowed $\mathcal{F}t$ value for ^{74}Rb using the Hartree-Fock $\delta_{C2} = 1.29(16)\%$ [2] correction is $\mathcal{F}t_{\rm HF} = 3082.2(65)_{ft}(36)_{\delta'_R}(9)_{\delta_{\rm NS}}(53)_{\delta_C}$ s $= 3082(9)$ s. Currently, the uncertainty in the experimental ft value is comparable to the uncertainty from the δ_C correction terms. However, the expected increase in the precision of the Q-value measurement in the near future will result in a situation in which the uncertainty in the corrected $\mathcal{F}t$ value for ^{74}Rb becomes dominated entirely by the uncertainty in the current isospin-symmetry-breaking corrections. Experimental guidance for improving these calculations is therefore essential and is discussed in the following sections in terms of both the overall δ_C correction and its δ_{C1}^n components.

As can be seen from Fig. 13, the superallowed $\mathcal{F}t$ values from $Z = 6$ to $Z = 37$ continue to strongly support the CVC hypothesis at the level of 1.3 parts in 10^4. Thus, if we assume that the CVC hypothesis is valid we can perform an internal consistency check on the δ_C corrections. The "experimental" isospin-symmetry-breaking correction for the β decay of ^{74}Rb was determined by enforcing CVC with the average $\overline{\mathcal{F}t}_{\rm WS} = 3072.34(75)$ [2,5,16] determined from the 12 precision cases other than ^{74}Rb via

$$\begin{aligned}\delta_C^{\rm exp}(^{74}\text{Rb}) &= 1 + \delta_{\rm NS} - \frac{\overline{\mathcal{F}t}_{\rm WS}}{ft(1+\delta'_R)},\\ &= 1.74(2)_{\overline{\mathcal{F}t}}(6)_{ft}(12)_{\delta'_R}(3)_{\delta_{\rm NS}}\%,\\ &= 1.74(14)\%,\end{aligned} \tag{8}$$

while the value of $\delta_C^{\rm exp}(^{74}\text{Rb})$ obtained using the average $\overline{\mathcal{F}t}_{\rm HF} = 3071.50(88)$ [2,5,16] from the other 12 precision cases with the Hartree-Fock δ_{C2} corrections was 1.76(14)%. These values, which represent a test of the large isospin-symmetry-breaking predicted in ^{74}Rb to ~8% of its own value, are to be compared with the theoretical values $\delta_C^{\rm WS} = 1.63(24)\%$ and $\delta_C^{\rm HF} = 1.42(17)\%$, showing excellent self-consistency within the Woods-Saxon calculations, but less so in the Hartree-Fock calculations.

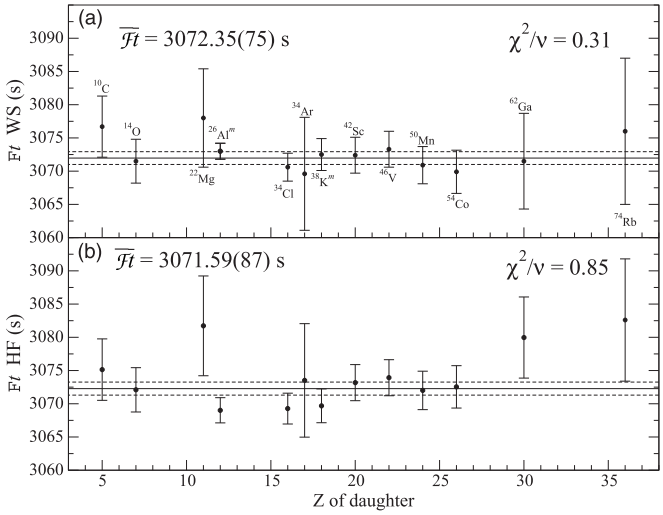

FIG. 13. A comparison of the superallowed $\mathcal{F}t$ value for ^{74}Rb obtained with the branching ratio from this work with the 12 other most precisely determined superallowed $\mathcal{F}t$ values using (a) Woods-Saxon radial wave functions for δ_{C2} and (b) the Hartree-Fock δ_{C2} values. The data are taken from Refs. [2,5,16,41,45] and the present work.

B. The isospin-symmetry-breaking terms δ^1_{C1}, δ^2_{C1}, $\delta^{(3)}_{C1}$, $\delta^{(4)}_{C1}$

An additional, and particularly demanding, test of the theoretical isospin-symmetry-breaking corrections was performed using the nonanalog Fermi branching-ratio measurements from this work, thereby constraining the isospin-configuration-mixing components δ^n_{C1}. The shell-model calculations described above that were used to predict the Gamow-Teller feeding also predict that 80% of the nonanalog Fermi β decay of ^{74}Rb will be concentrated in the first two excited 0^+ states with nonanalog Fermi β-decay branching ratios of 360 and 228 ppm, respectively. The tentatively assigned (0^+_3) and (0^+_4) states, with excitation energies of 2173 and 2573 keV agree very well with the theoretical excitation energies of 2210 and 2570 keV and are predicted to have very weak nonanalog Fermi branches of 13 and 6 ppm, respectively.

Using Eq. (4), direct tests of the δ^n_{C1} terms for these states were performed. By combining the ratio of the phase space integrals $(f_0/f_1) = 1.3$ and the upper limit of the nonanalog Fermi β-decay branch of 159(58) ppm for the first excited 0^+_1 state gives a firm upper limit on the δ^1_{C1} correction of $\delta^1_{C1} \leqslant 0.021(8)\%$, which is consistent with the adopted Towner and Hardy value of 0.050(30)% [17]. However, it should be noted that this experimental upper limit assumes zero unobserved γ feeding into the 0^+_1 state from above. To estimate the unobserved γ feeding, we again turn to theory. As shown in Table V, the shell-model calculations predict that approximately 16% of the γ-ray intensity from 1^+ states above 1742 keV feeds the 0^+_1 state. The calculation which best reproduced many aspects of the ^{74}Rb decay scheme, including the the total non-superallowed β branching ratio, was the calculation with $g_{A_{\rm eff}} = 0.72$ and the lowest 1^+ state at the experimental value of 3.337 MeV. This calculation was adjusted to closely reproduce the experimental intensity of the $2^+_1 \rightarrow 0^+_{\rm gs}$ transition. However, as can be seen in Table V, the predicted absolute γ-ray feeding from above 1742 keV also reproduces the measured $I_{\rm out} - I_{\rm in}$ values for the 2^+_2 and 2^+_3 states to within 15% and 34%, respectively. We therefore use the conservative estimate that the calculated γ-ray feeding into the excited 0^+ states from states above 1742 keV are accurate to $\pm$40%. We thereby estimate the nonanalog Fermi feeding into the excited 0^+ states by subtracting the predicted unobserved γ-ray feeding intensity from the observed $I_{\rm out} - I_{\rm in}$ (see Tables I, II, and V).

If we apply the above prescription to the 0^+_1 state, the observed γ-ray feeding into the 0^+_1 state from states above 1742 keV is 394(33) ppm and the predicted γ-ray feeding into the 0^+_1 state is 663(265) ppm. The unobserved γ-ray intensity was therefore estimated to be 269(267) ppm. Subtracting the unobserved γ-ray intensity from $I_{\rm out} - I_{\rm in} = 159(58)$ gives an estimate for the intensity of the nonanalog Fermi β-decay branch of $-110(269)$ppm. Clearly, a negative β-branching ratio is unphysical, but this calculation indicates that the unobserved γ-ray feeding from above likely accounts for the majority of the measured $I_{\rm out} - I_{\rm in}$ intensity for the 0^+_1 state, with a very small, if any, nonanalog Fermi β-feeding component. We interpret this result as a 1σ upper limit of $\leqslant$159 ppm on the Fermi β feeding, which is less than half of the predicted nonanalog Fermi β feeding to the first excited 0^+_1 state of 360 ppm. Using Eq. (4), the corresponding upper limit on the isospin-symmetry-breaking correction is $\delta^1_{C1} \leqslant 0.021\%$, at the lower end of the uncertainty range on the predicted value of 0.050(30) [17]%.

In a similar manner, the nonanalog Fermi feeding and corresponding δ^n_{C1} values were determined for the 0^+_2, (0^+_3) and (0^+_4) levels. The results are summarized in Table VII. It is

TABLE VII. A summary of the constraints set on the isospin-symmetry-breaking terms δ^n_{C1} in ^{74}Rb decay. The adopted theoretical values of δ^n_{C1} are from Ref. [17] and were assigned a common uncertainty of 0.03%.

E	$(\frac{f_0}{f_n})$	Experiment	Theory	Experiment		Theory	
(keV)		GT + F (ppm)	GT[a,b] (ppm)	F (ppm)	δ^n_{C1} (%)	F (ppm)	δ^n_{C1} (%)
509	1.30	553(49)	663(265)	$\leqslant$159	$\leqslant$0.021	360	0.050(30)
1654	2.50	518(13)	199(80)	319(81)	0.080(20)	228	0.060(30)
2173	3.47	141(8)	183(73)	$\leqslant$32	$\leqslant$0.011	13	0.005(30)
2537	4.73	140(8)	89(36)	51(37)	0.024(16)	6	0.003(30)

[a] $g_{A_{\rm eff}} = 0.72$.
[b] Uncertainty of 40% was assigned to the absolute γ-ray feeding from above into each excited 0^+ state predicted by the shell-model calculations.

interesting to note that the upper limit on the total nonanalog Fermi β feeding to the 0_1^+–0_4^+ states of 663 ppm deduced in this work is comparable to the theoretical prediction of 607 ppm and the resulting sum of $\delta_{C1}^{1-4} = 0.104(35)\%$ is also comparable to the theoretical sum $\delta_{C1}^{1-4} = 0.118(60)\%$. There are, however, differences between experiment and theory in the state-by-state pattern of the nonanalog Fermi β feeding, particularly for the first two excited 0^+ states where the experimental results indicate little, if any, β feeding to the first excited 0^+ state and the majority of the nonanalog Fermi β feeding concentrated on the second excited 0^+ state at 1654 keV. Our interpretation of the above state-by-state comparisons of the δ_{C1} corrections is that the current shell-model calculations have difficulty describing the detailed wave functions of the 0^+ states. In particular, the 0_1^+ nanosecond isomer at an excitation energy of 509 keV in ^{74}Kr has been interpreted as evidence of prolate-oblate shape coexistence in this mass region [40], consistent with the large $\rho^2(E0)$ matrix element we report in Sec. III C. This state is likely to have very little overlap with the 0^+ ground state of ^{74}Rb, which corresponds to the analog of the ^{74}Kr ground state, leading to the small nonanalog Fermi branch to the 0_1^+ state determined in this experiment. The accurate description of such states with vastly different intrinsic shapes is generally beyond the capabilities of the shell-model calculations performed in this region to date. The current shell-model calculations, for example, using a ^{56}Ni core with 18 nucleons distributed among the $p_{3/2}$, $f_{5/2}$, and $p_{1/2}$ orbitals would place the first excited 0^+ state of ^{74}Kr at 2 MeV excitation energy. To reproduce the observed low-lying 0_1^+ state in ^{74}Kr, the $g_{9/2}$ and $d_{5/2}$ orbitals were added to the model space, the number of configurations were truncated to the low-seniority states, and the strength of the cross-shell matrix elements was increased [38]. This prescription successfully lowers the excitation energy of the first excited 0^+ state and produces a spectrum of 0^+ states in reasonable agreement with experiment. The state-by-state comparison of the δ_{C1}^n values, however, suggest that the detailed wave functions of these 0^+ states are not being accurately reproduced in the current shell-model calculations.

V. CONCLUSION

A high-precision branching ratio measurement was performed for the superallowed β decay of ^{74}Rb using the 8π spectrometer at TRIUMF. In this experiment, 23 excited states were identified in ^{74}Kr following the β decay of ^{74}Rb. A total of 58 γ-ray and conversion-electron transitons were placed in the decay scheme following $8.241(4) \times 10^8$ detected β decays of ^{74}Rb. An observed non-superallowed branch of 0.395(7)% was determined from the intensities of the identified γ rays and conversion electrons feeding the ground state, while the unobserved γ-ray feeding to the ground state was estimated to be 0.060(30)%, leading to a superallowed branching ratio of $B_0 = 99.545(31)\%$. The superallowed branching ratio is now the most precise experimental quantity in the determination of the superallowed ft value of ^{74}Rb. Combining the world-average half-life and Q value measurements for ^{74}Rb with the measured superallowed branching ratio reported here leads to a superallowed ft value of 3082.8(65) s, with an uncertainty that is expected to be significantly reduced in the near future through a reduction in the uncertainty of the Q value [41].

Tests of the model-dependent isospin-symmetry-breaking correction δ_C were performed by comparing the ft value of this work with the world-average $\overline{\mathcal{F}t}$ value of the other 12 precisely measured superallowed decays. The application of the Woods-Saxon radial overlap corrections of Ref. [5] and the shell-model δ_{C1} values of Ref. [17] to the superallowed data continues to provide an impressive confirmation of the CVC hypothesis. Furthermore, demanding tests of the isospin-symmetry-breaking components δ_{C1}^1, δ_{C1}^2, $\delta_{C1}^{(3)}$, and $\delta_{C1}^{(4)}$ were performed based on the measured nonanalog Fermi β-decay branches to these states. These state-by-state comparisons suggest that the current shell-model calculations have difficulty accurately describing the wave functions of the 0^+ states in this region of strong nuclear deformation, shape coexistence and rapid shape transitions [37,40,46,47]. The current results will help constrain future calculations of the configuration mixing component of the isospin-symmetry-breaking corrections in this mass region.

ACKNOWLEDGMENTS

This work has been partially supported by the Natural Sciences and Engineering Research Council of Canada. TRIUMF receives federal funding via a contribution agreement with the National Research Council of Canada.

[1] J. C. Hardy and I. S. Towner, Phys. Rev. C **71**, 055501 (2005).
[2] J. C. Hardy and I. S. Towner, Phys. Rev. C **79**, 055502 (2009).
[3] I. S. Towner and J. C. Hardy, Rep. Prog. Phys. **73**, 046301 (2010).
[4] W. J. Marciano and A. Sirlin, Phys. Rev. Lett. **96**, 032002 (2006).
[5] I. S. Towner and J. C. Hardy, Phys. Rev. C **77**, 025501 (2008).
[6] E. Blucher *et al.*, arXiv:hep-ph/0512039.
[7] A. Czarnecki, W. J. Marciano, and A. Sirlin, Phys. Rev. D **70**, 093006 (2004).
[8] G. A. Miller and A. Schwenk, Phys. Rev. C **78**, 035501 (2008).
[9] N. Auerbach, Phys. Rev. C **79**, 035502 (2009).
[10] H. Liang, N. V. Giai, and J. Meng, Phys. Rev. C **79**, 064316 (2009).
[11] A. E. Çalik, M. Gerçeklioğlu, and D. I. Salamov, Z. Naturforsch. A **64**, 865 (2009).
[12] G. A. Miller and A. Schwenk, Phys. Rev. C **80**, 064319 (2009).
[13] G. F. Grinyer, C. E. Svensson, and B. A. Brown, Nucl. Instrum. Methods Phys. Res., Sect. A **622**, 236 (2010).
[14] I. S. Towner and J. C. Hardy, Phys. Rev. C **82**, 065501 (2010).
[15] W. Satuła, J. Dobaczewski, W. Nazarewicz, and M. Rafalski, Phys. Rev. Lett. **106**, 132502 (2011).
[16] P. Finlay *et al.*, Phys. Rev. Lett. **106**, 032501 (2011).
[17] I. S. Towner and J. C. Hardy, Phys. Rev. C **66**, 035501 (2002).

[18] J. C. Hardy, L. C. Carraz, B. Jonson, and P. G. Hansen, Phys. Lett. B **71**, 307 (1977).
[19] A. Piechaczek *et al*., Phys. Rev. C **67**, 051305 (2003).
[20] B. Hyland *et al*., Phys. Rev. Lett. **97**, 102501 (2006).
[21] P. Finlay *et al*., Phys. Rev. C **78**, 025502 (2008).
[22] E. Hagberg, V. T. Koslowsky, J. C. Hardy, I. S. Towner, J. G. Hykawy, G. Savard, and T. Shinozuka, Phys. Rev. Lett. **73**, 396 (1994).
[23] P. Bricault, P. Schmor, G. Stanford, C. Mark, M. Dombsky, M. Gallop, L. Moritz, and L. Udy, in *Proceedings of the 15th International Conference on Cyclotrons and Their Applications (Cyclotrons '98)* (Institute of Physics Publishing, Caen, France, 1999), p. 347.
[24] M. Dombsky *et al*., Rev. Sci. Instrum. **69**, 1170 (1998).
[25] M. Dombsky *et al*., Rev. Sci. Instrum. **71**, 978 (2000).
[26] G. C. Ball *et al*., Phys. Rev. Lett. **86**, 1454 (2001).
[27] C. E. Svensson *et al*., Nucl. Instrum. Methods Phys. Res., Sect. B **204**, 660 (2003).
[28] D. C. Camp, D. R. Fielder, and B. P. Foster, Nucl. Phys. A **163**, 145 (1971).
[29] H. W. Taylor, R. L. Schulte, P. J. Tivin, and H. Ing, Can. J. Phys. **53**, 107 (1975).
[30] G. C. Ball *et al*., J. Phys. G **31**, S1491 (2005).
[31] S. Raman, C. Yonezawa, H. Matsue, H. Iimura, and N. Shinohara, Nucl. Instrum. Methods Phys. Res., Sect. A **454**, 389 (2000).
[32] Z. Kis, B. Fazekas, J. Östör, Z. Révay, T. Belgya, G. L. Molnár, and L. Koltay, Nucl. Instrum. Methods Phys. Res., Sect. A **418**, 374 (1998).
[33] I. M. Band, M. B. Trzhaskovskaya, C. W. Nestor Jr., P. O. Tikkanen, and S. Raman, At. Data Nucl. Data Tables **81**, 1 (2002).
[34] E. L. Church and J. Wesner, Phys. Rev. **103**, 1035 (1956).
[35] D. A. Bell, C. E. Aveledo, M. G. Davidson, and J. P. Davidson, Can. J. Phys. **48**, 2542 (1970).
[36] A. Passoja and T. Salonen, *Electronic Factors for K-Shell-Electron Conversion Probability and Electron-Positron Pair Formation Probability in Electric Monopole Transitions* (1986), JYFLRR-2/86, http://www.ntis.gov/search/product.aspx?ABBR=DE87753040.
[37] W. Korten *et al*., Nucl. Phys. A **752**, 255 (2005).
[38] J. C. Hardy and I. S. Towner, Phys. Rev. Lett. **88**, 252501 (2002).
[39] D. N. Poenaru, R. A. Gherghescu, and W. Greiner, J. Phys. G: Nucl. Part. Phys. **39**, 015105 (2012).
[40] E. Bouchez *et al*., Phys. Rev. Lett. **90**, 082502 (2003).
[41] S. Ettenauer *et al*., Phys. Rev. Lett. **107**, 272501 (2011).
[42] A. Kellerbauer *et al*., Phys. Rev. Lett. **93**, 072502 (2004).
[43] A. Kellerbauer *et al*., Phys. Rev. C **76**, 045504 (2007).
[44] M. Oinonen *et al*., Phys. Lett. B **511**, 145 (2001).
[45] E. Mané *et al*., Phys. Rev. Lett. **107**, 212502 (2011).
[46] C. D. O'Leary *et al*., Phys. Rev. C **67**, 021301 (2003).
[47] J. J. Valiente-Dobón *et al*., Phys. Rev. Lett. **95**, 232501 (2005).